Structure of sticky-hard-sphere random aggregates: The viewpoint of contact coordination and tetrahedra

M. Blétry,* V. Russier, and E. Barbé
Université Paris Est, ICMPE (UMR 7182), CNRS, UPEC, F-94320 Thiais, France

J. Blétry
Universidad Nacional del Sur, Bahia Blanca, 8000FTN Buenos Aires, Argentina

(Received 12 January 2018; revised manuscript received 16 May 2018; published 2 July 2018)

We study more than 10^4 random aggregates of 10^6 monodisperse sticky hard spheres each, generated by various static algorithms. Their packing fraction varies from 0.370 up to 0.593. These aggregates are shown to be based on two types of disordered structures: random regular polytetrahedra and random aggregates, the former giving rise to δ peaks on pair distribution functions. Distortion of structural (Delaunay) tetrahedra is studied by two parameters, which show some similarities and some differences in terms of overall tendencies. Isotropy of aggregates is characterized by the nematic order parameter. The overall structure is then studied by distinguishing spheres in function of their contact coordination number (CCN). Distributions of average CCN around spheres of a given CCN value show trends that depend on packing fraction and building algorithms. The radial dependence of the average CCN turns out to be dependent upon the CCN of the central sphere and shows discontinuities that resemble those of the pair distribution function. Moreover, it is shown that structural details appear when the CCN is used as pseudochemical parameter, such as various angular distribution of bond angles, partial pair distribution functions, Ashcroft-Langreth and Bhatia-Thornton partial structure factors. These allow distinguishing aggregates with the same values of packing fraction or average tetrahedral distortion or even similar global pair distribution function, indicative of the great interest of paying attention to contact coordination numbers to study more precisely the structure of random aggregates.

DOI: 10.1103/PhysRevE.98.012101

I. INTRODUCTION

Random aggregates (RA) of monodisperse spheres are of great interest to simulate various physical systems, such as amorphous solids, liquids, powders, etc. In particular, a fine characterization of their local or longer range structural properties is of interest to classify the various types of random aggregates of spheres that can exist and study their properties.

Many different approaches allow building random aggregates of spheres. Broadly, they may be divided into two categories. The first one consists of algorithms for which all spheres are introduced at once and then the system relaxes towards some more or less disordered structural state (e.g., molecular dynamics [1], the Lubachevsky-Stillinger algorithm [2], the Jodrey-Tory algorithm [3], or Monte Carlo relaxation of chains of hard sphere [4]). This family of algorithms produces aggregates whose properties mimic what was found in many disordered systems, notably, the dependence of the contact coordination number with packing fraction, and they are also able to produce aggregates with packing fraction equal to or even superior to the random-close-packing (RCP) value $\gamma_{RCP} \approx 0.64$ or equal to or lower than the random-loose-packing (RLP) value $\gamma_{RLP} \approx 0.555$ (see [5]). However, γ_{RLP} presents a strong dependence on interparticle interactions [6], which suggests that no geometrical property must be associated with the RLP transition, whereas the RCP state might have structural or geometrical constraints that set an upper bound to γ_{RCP}, such as the proportion of spheres involved in quasiperfect tetrahedra, as observed by Anikeenko and Medvedev [7].

The second large category of algorithms introduces spheres in the aggregate one by one and sets their position definitely at once (see, e.g., [8]). Aggregates built by such methods have two important differences from those of the first category: First, their average contact coordination number remains close to 6; second, it is impossible to produce aggregates with packing fraction higher than 0.6. Hence, the latter family of algorithms gives access to random aggregates with somewhat different structural properties from the former. Moreover, using sticky hard spheres, contact neighbors are rigorously defined by Dirac δ functions and this allows studying various properties related to the coordination number of spheres in a simple and unambiguous manner.

In [9], a study of several hundred sequentially built aggregates was conducted. It was found that for the lowest packing fractions, δ peaks appear on the pair distribution function, which corresponds to the formation of a disordered polytetrahedral structure in the random-packing aggregate.

The present study extends the results obtained in [9] by looking at structural tetrahedra, isotropy, contact coordination numbers, partial distribution functions, and partial structure factors, corresponding to pairs of spheres with equal or different contact coordination numbers. It also introduces a family of random aggregates formed by spheres added

*Corresponding author: bletry@icmpe.cnrs.fr

in regular building tetrahedra, which appears essential to understand the composite nature of other sequentially built random aggregates.

II. STUDIED AGGREGATES

More than 10 000 aggregates, each one containing 10^6 spheres with radius $r_s = 1$ (and hence diameter $d = 2$), were built and studied.[1] They fall into two broad families: random irregular polytetrahedral aggregates (RIPAs) and random regular polytetrahedral aggregates (RRPAs). All of them were built by adding spheres one by one at their final position, tangentially to three existing ones.

A. Random irregular polytetrahedral aggregates

Most aggregates were of RIPA type. They were built using algorithms that have been presented in detail in [9] and are only summarized here. A seed of three spheres forming an equilateral triangle is used. Each new sphere P is positioned tangentially to at least three already present spheres (noted O, A, and B). The new sphere can be introduced in a hole whose size is maximized (MAX algorithms) or chosen randomly (RAN algorithms) in the vicinity of the local origin O, itself chosen randomly in the aggregate. Moreover, it is possible to insert from 1 up to 9 spheres at once (according to the index N_{ins}, the number of spheres inserted) around a given origin O (algorithms MAX-1 to MAX-9 and RAN-1 to RAN-9). Finally, the neighborhood explored to choose spheres A and B around O is a cube whose edge length a can be varied: It controls strongly the packing fraction of the aggregates. The larger the value of a, the higher the packing fraction. It is varied between about 3.4 and 8 as, for $a < 3.4$, no aggregate can be generated and for $a > 8$, the maximum packing fraction is reached and no evolution of the generated aggregates is noted for higher values of a (see Fig. 2 in [9]). More than 300 aggregates of 10^6 spheres were built, by varying a for each family of these algorithms.

An additional modification with regard to the aggregates studied in [9] was to choose the origin O as close as possible to the center (0,0,0) of the growing aggregate (RMIN algorithms), instead of in a purely random fashion. This change has the effect of increasing the maximum packing fraction, reached for MAX-1 and $a > 3.5$, of about 1%, from 0.586 to 0.593. All other aggregates generated by RMIN-MAX algorithms have a slightly higher packing fraction than their MAX counterparts (i.e., same values of a and N_{ins}) with no significant changes concerning the structural results presented in [9]. This modification also allows for a more homogeneous growth of the aggregate. Only the results obtained for RMIN-MAX-1 will be used hereafter.[2]

Finally, as it turned out that the previous families of aggregates had some inhomogeneities of their packing fraction close to (0,0,0), some aggregates were generated by using as the seed a set of N spheres taken in previously built aggregates, instead of an equilateral triangle (N-RMIN-MAX-1 algorithm). The positions of the spheres composing the seed are taken from an aggregate with the same values of other parameters (a and N_{ins}), far from the origin (0,0,0), which has the effect to remove the central area with higher packing fraction. Typically, the number of spheres in the seed is between 30 and 600. However, this modification entails only slight changes of pair distribution functions or structure factors.

B. Random regular polytetrahedral aggregates

The other algorithm that has been used produces aggregates with only regular building tetrahedra [10]. In this case, the newly inserted sphere P forms a regular tetrahedron with the three already contacting spheres O, A, and B, i.e., $PO = PA = PB = OA = OB = AB = 2$. For these algorithms, a has virtually no impact on packing fraction, but the number of inserted spheres around a given local origin (N_{ins}) does.

Once again, the local origin O can be chosen at random, or as the closest one to the center of the aggregate. When it is chosen randomly (RRPA), the maximum packing fraction (0.418) is reached for $N_{\text{ins}} = 3$ and a minimum of 0.408 is observed for $N_{\text{ins}} = 1$ and beyond 4. When O is chosen as the closest possible origin from the aggregate center (RMIN-RRPA), the maximum packing fraction is 0.456 and is reached for $N_{\text{ins}} > 4$. Similar aggregates, so-called saturated polytetrahedra, have been studied by Medvedev and Pilyugina [11]. They found a packing fraction of 0.435 for aggregates consisting of about 576 000 spheres. This value falls in between the maximum ones obtained for aggregates choosing O randomly (lower bound) and those taking O as the closest sphere from the origin (higher bound). It should be noted that RIPAs and RRPAs distinguish aggregates based on their building algorithms, not their structure, which will be discussed in details below.

The isotropy and the randomness of all aggregates have been systematically checked through the distribution of i-j bonds and the nematic tensor formalism and turn out to be satisfactory. More details on the latter point are provided in the Appendix.

III. PACKING FRACTION

A. Basic relations

The radius R_m of a large spherical aggregate centered in (0,0,0) and made of N spheres centered in $\vec{R}_i$ is given to a good approximation by [10]

$$R_{\text{ag}} = \sqrt{R^2_{\text{quad}}}, \tag{1}$$

where R_{quad} is the average quadratic radius of all spheres in the aggregate

$$R^2_{\text{quad}} = \frac{5}{3}\frac{1}{N}\sum_{i=1}^{N} R_i^2. \tag{2}$$

However, finite aggregates are not fully spherical and exhibit local order oscillations. Therefore, their packing

[1] Hereafter, unless otherwise mentioned, all distances are expressed in r_s as the unit of length ($r_s = 1$). Similarly, r_s^{-1} is the unit in reciprocal space.

[2] Yet another family of algorithms has been developed for which the newly added sphere is positioned by controlling the value of the building tetrahedra distortion. However, this strategy leads to the exact same $P(r)$ as the one obtained for RA built with the positioning in function of the hole size and has the same maximum packing fraction; these aggregates will not be further studied here.

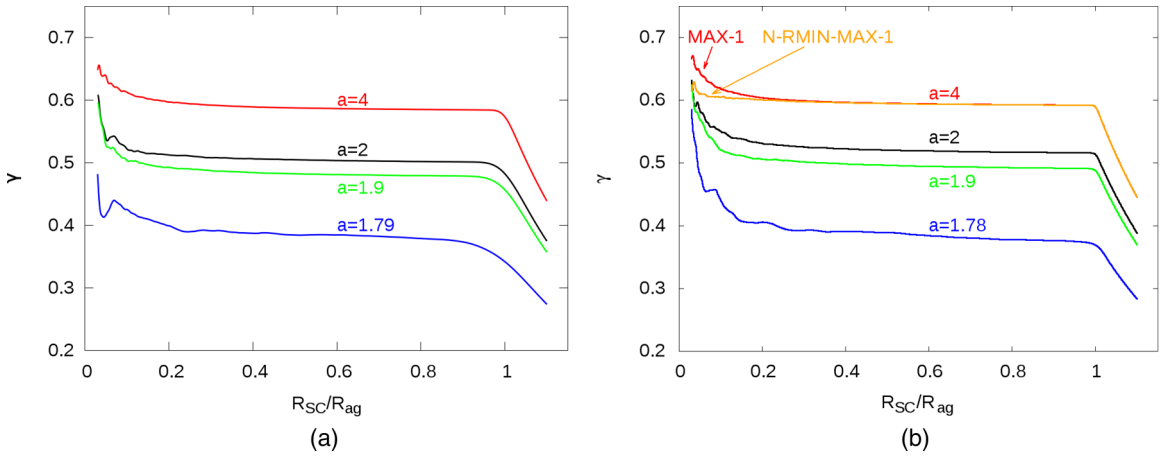

FIG. 1. The $\gamma(R_{SC}/R_{ag})$ for several (a) MAX-1 aggregates and (b) RMIN-MAX-1 aggregates built with various values of a and a single N-RMIN-MAX-1 aggregate (seed composed of 600 spheres), for the sake of comparison, with $\mathcal{S}$ centered in (0,0,0).

fraction varies as a function of the radius R_{SC} of the sphere cut into the aggregate bulk and deserves special attention.

The volume $V_s(r)$ shared by a sphere of radius $r_s = 1$ whose center is at a distance r from the origin (0,0,0) with another sphere $\mathcal{S}$, of radius R_{SC}, centered in (0,0,0) is [12]

$$V_s(r,R_{SC}) = \begin{cases} \frac{4}{3}\pi r_s^3, & r \leqslant R_{SC} - r_s \\ \pi \frac{(R_{SC}+r_s-r)^2\left(r^2+2rr_s-3r_s^2+2rR_{SC}+6R_{SC}r_s-3R_{SC}^2\right)}{12r}, & R_{SC}-r_s < r < R_{SC}+r_s \\ 0, & r \geqslant R_{SC}+r_s. \end{cases} \tag{3}$$

These relationships can also be used for any sphere $\mathcal{S}$ centered in x, y, and z by a mere change of reference frame. Hence, the packing fraction of the sphere $\mathcal{S}$ can be directly determined for any radius R_{SC} as

$$\gamma(R_{SC}) = \frac{\sum_{i=1}^{N} V_s(r_i,R_{SC})}{\frac{4}{3}\pi R_{SC}^3}, \tag{4}$$

where i accounts for all spheres in the aggregate. Finally, it is possible to determine the packing fraction of shells of arbitrary thickness $w = R_o - R_i$, where R_i is the inner radius and R_o the outer radius of the shell, simply by removing the portion of spheres outside of the shell, according to the volume complementary of the relation (3).

B. Packing fraction of spheres inscribed in the aggregate

The evolution of the packing fraction of spheres inscribed in the aggregate as a function of their radius $\gamma = f(R_{SC}/R_{ag})$ (Fig. 1) shows that, for all aggregates, whatever their building algorithm, the packing fraction decreases slightly when R_{SC} increases. A seed effect appears as for MAX-1 and RMIN-MAX-1 aggregates (three spheres forming an equilateral triangle as the seed), a first regime of fast decrease is observed for $R_{SC} < 0.2R_{ag}$, i.e., for a number of spheres below approximately 8000, and then the packing fraction tends to plateau, whereas for N-RMIN-MAX-1 aggregates (the seed consisting of spheres taken far from the origin in a previously generated aggregate), this initial decrease is much faster. Nevertheless, the exact range of effect of the seed can only be asserted by the packing fraction of shells studied hereafter.

This effect probably stems from the fact that contacting equilateral-triangle configurations are extremely rare in high-packing-fraction aggregates. As a matter of fact, this seed dependence disappears for lower-packing-fraction aggregates, in which such configurations are rather frequent. On the other hand, N-RMIN-MAX-1 and RMIN-MAX-1 aggregates show exactly the same behavior for larger values of R_{SC}.

For every aggregate, a second regime is observed when $R_{SC} \to R_{ag}$, i.e., when $\mathcal{S}$ reaches the limit of the aggregate: Logically, the packing fraction decreases faster. For a perfectly spherical aggregate, when $R_{SC} > R_{ag} + r_s$, then the packing fraction of $\mathcal{S}$ should decrease as R_{SC}^{-3}. When this decrease is at first more progressive, it shows that the aggregate has an imperfect shape and either has protuberances on its surface or is not overall perfectly spherical.

For the same value of a, RMIN-MAX-1 aggregates tend to have a higher packing fraction than the corresponding MAX-1 aggregates, as well as a sharper decrease of γ when $R_{SC} \to R_{ag}$, which shows that RMIN-MAX-1 aggregates have a more regular surface than MAX-1 aggregates. For the latter, the thickness of the imperfect aggregate is about $1.5d$ for $a = 3.5$ ($\gamma = 0.586$) and about $5d$ for $a = 1.79$ ($\gamma = 0.370$). For RMIN-MAX-1 aggregates, the thickness of the imperfect aggregate is roughly $d/4$ for $a = 3.5$ ($\gamma = 0.593$) and about $1.5d$ for $a = 1.78$ ($\gamma = 0.378$).

C. Packing fraction of shells

Figures 2(a) and 2(b) represent the variation of packing fraction in shells with thickness $w = 0.1$ for the densest aggregates produced by algorithms MAX-1, RMIN-MAX-1,

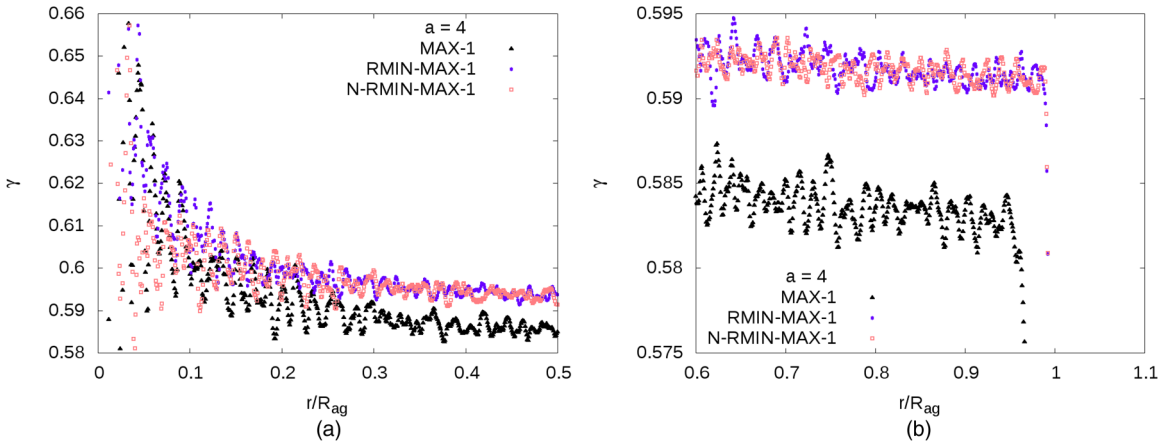

FIG. 2. Packing fraction of shells with thickness $w = 0.1r_s$ on the densest aggregates built with three strategies: MAX-1 (three-sphere seed), RMIN-MAX-1 (three-sphere seed, RMIN), and N-RMIN-MAX-1 with a spherical seed of radius 10 extracted from a previously generated aggregate with the same value for a and N_{ins} for (a) relatively small r ($r/R_{\text{ag}} \in [0,0.5]$) and (b) large r ($r/R_{\text{ag}} \in [0.5,1]$).

and N-RMIN-MAX-1. Globally, the packing fraction of such shells oscillates with r. Its average value decreases from a higher value near the seed to a smoother behavior when r increases. The N-RMIN-MAX-1 aggregate presents virtually no effect of the seed: The packing fraction of shells reaches the average behavior for very small values of r, which seems logical as for these aggregates the seed consists of a set of spheres with the average structure. The RMIN-MAX-1 and N-RMIN-MAX-1 aggregates converge for $r \in [0.1R_{\text{ag}}, 0.15R_{\text{ag}}]$: The effect of the initial equilateral-triangle seed of RMIN-MAX-1 aggregates seems then to act on about 10^3 spheres in the whole aggregate, consisting of 10^6 spheres, i.e., significantly less than suggested above by the comparison, in Fig. 1(b), of $\gamma = f(R_{\text{SC}}/R_{\text{ag}})$ for the two same aggregates. Figure 3 compares two aggregates built by RMIN-MAX-1 and N-RMIN-MAX-1 algorithms, where spheres are colored based on their contact coordination number (CCN). It appears that the former aggregate has a brighter atypical central area in the region of the seed, denoting unusual structural properties with respect to the rest of the aggregate, whereas the latter displays a seed area much more similar to the rest of the aggregate.

Moreover, for aggregates with lower packing fraction (i.e., for aggregates built using lower values of a and in which regular polytetrahedra appear), the range of aggregates affected by the seed decreases and completely disappears for the lowest-packing-fraction aggregates. In that case, indeed, the structure contains a significant amount of equilateral triangles and the initial seed ceases to be special in comparison with the rest of the structure. At large values of r [Fig. 2(b)], oscillations can still be detected in the packing fraction of shells, however with a much smaller amplitude. A slight decrease of the average value is noticeable: The farther a shell is from the center of the aggregate, the lower its packing fraction is, on average. The origin of this phenomenon is not obvious to us. For $r > R_{\text{ag}}$, the packing fraction of shells falls rapidly to 0.

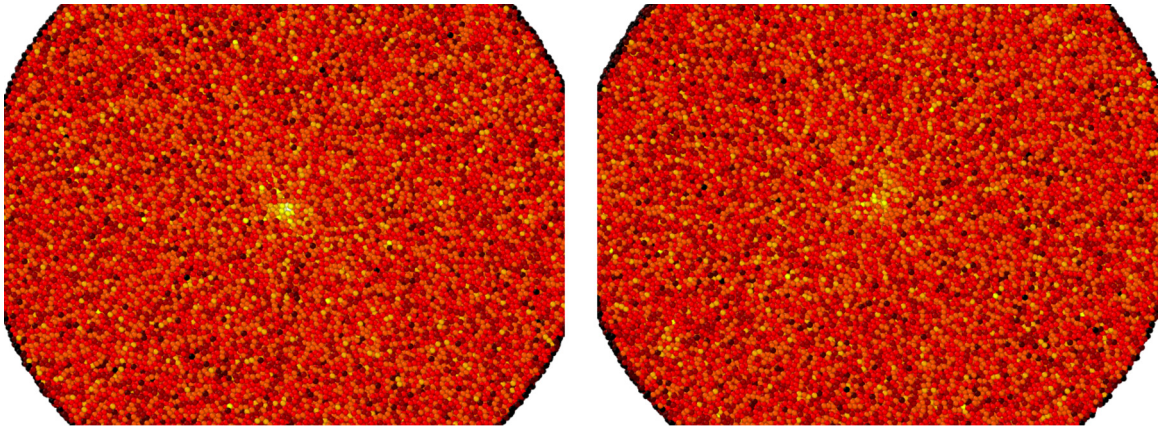

FIG. 3. Slices of aggregates generated by two algorithms: (a) RMIN-MAX-1 with $a = 4$ and (b) N-RMIN-MAX-1 with $a = 4$ and a seed consisting of $N = 400$ spheres. Colors (grayscale) correspond to the contact coordination number: Brighter spheres have a higher CCN. (These figures were generated with OVITO software [13].)

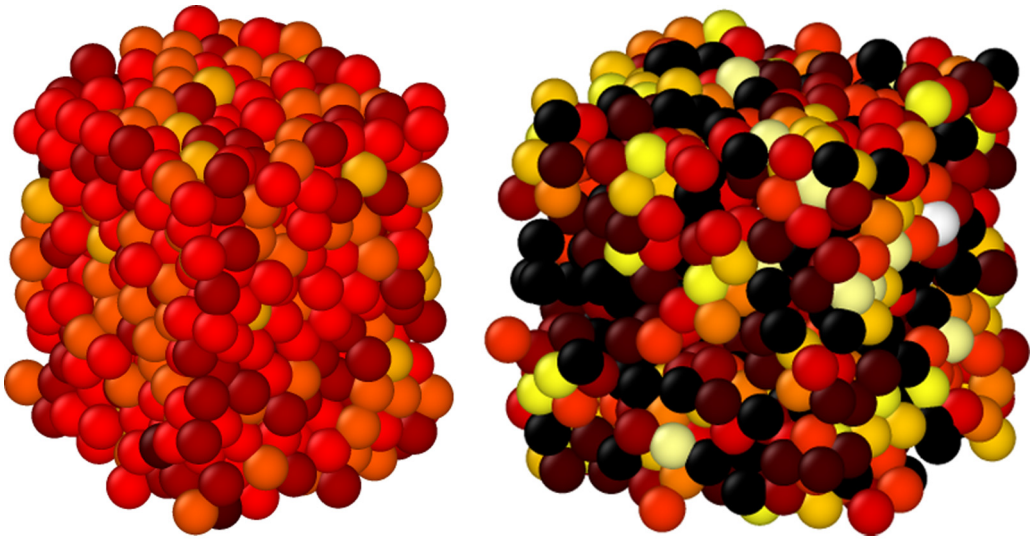

FIG. 4. Slices of aggregates generated by two algorithms: (a) RMIN-MAX-1 with $a = 4$ and (b) RRPA. Colors (grayscale) correspond to the contact coordination number: Brighter spheres have a higher CCN. (These figures were generated with OVITO software [13].)

IV. TETRAHEDRAL STRUCTURE

The structure of random packings of spheres is commonly assessed via the tetrahedra connecting sphere centers, forming the so-called Delaunay tessellation [14] (these tetrahedra are noted by the subscript D in what follows). For the present study, Delaunay tessellations were built using the CGAL library [15,16].

In [9], another type of tetrahedra was studied, called building tetrahedra (denoted by the subscript BT hereafter). A building tetrahedron is formed by spheres O, A, B, and P when adding the new sphere P tangentially to the three other ones, O, A, and B. It should be noted that such tetrahedra may or may not belong to Delaunay's tessellation. The distortion of building tetrahedra was shown to be a very significant structural parameter, allowing the correlation of various structural traits of the aggregates. In this section, we focus on two distortion parameters of Delaunay tetrahedra.

A. Distortion parameters

The first tetrahedral distortion parameter has been defined for the characterization of building tetrahedra [9] by the relation

$$\kappa_{\mathrm{BT}} = \frac{3d^2 + OA^2 + OB^2 + AB^2}{6d^2}, \tag{5}$$

where O, A, and B are the three sphere centers used to add the new sphere P and the term $3d^2$ corresponds to the three necessary sphere contacts PO, PA, and PB imposed to building tetrahedra by the algorithm. The maximum value of κ_{BT} is 2 and is obtained for a centered equilateral triangle with side $d\sqrt{3}$ of three spheres, with the additional sphere P at its barycenter, while the κ_{BT} minimum value, 1, corresponds to a regular tetrahedron.

The definition of the parameter κ_{BT} is immediately extended to Delaunay tetrahedra by the relation

$$\kappa_D = \sum_i \sum_{j>i} \frac{d_{ij}^2}{6d^2}, \tag{6}$$

where i and j are the vertices of the tetrahedron and d_{ij} is the vertex length. The smallest distance possible between sphere centers is $d_{ij} = d = 2$, hence the smallest possible value is obtained for a regular tetrahedron and is $\kappa_D = 1$.

The last distortion parameter to be studied hereafter is the longest edge length L_{max} of the considered tetrahedron. The smallest possible value of L_{max} is d, which is found in the case of a regular tetrahedron. The behavior of L_{max} has already been studied, along with others, notably by Anikeenko *et al.* [17] on aggregates built using the Jodrey-Tory (JT) algorithm [3] and the Lubachevsky-Stillinger (LS) algorithm [2,18]. Anikeenko *et al.* [17] found that L_{max}, in spite of its simplicity, shows great consistency when compared with two other parameters, namely, the edge differences and the procrustean distance.

B. Distributions of distortion parameters

Globally, the distribution of distortion parameters suggests that two limiting aggregates exist, the densest one, produced by (RMIN)-MAX-1 algorithms (here for $\gamma = 0.586$) and the RRPA. The first limiting aggregate will be called a fully random (FR) component and the second one a regular polytetrahedral (RP) component. The terms FR and RP components refer to structural traits of the aggregates studied here. As a matter of fact, RRPAs are fully RP, whereas RIPAs may share features of these two basic components in a variable proportion, depending on their packing fraction and building algorithm. Figure 4 shows local structures of the RIPA with the smallest proportion of RP component [Fig. 4(a)] and a RRPA [Fig. 4(b)]. The RRPA presents larger holes in the structure, however the polytetrahedral nature of the latter is quite difficult to visualize. On the other hand, it is clear that the RIPA with high packing

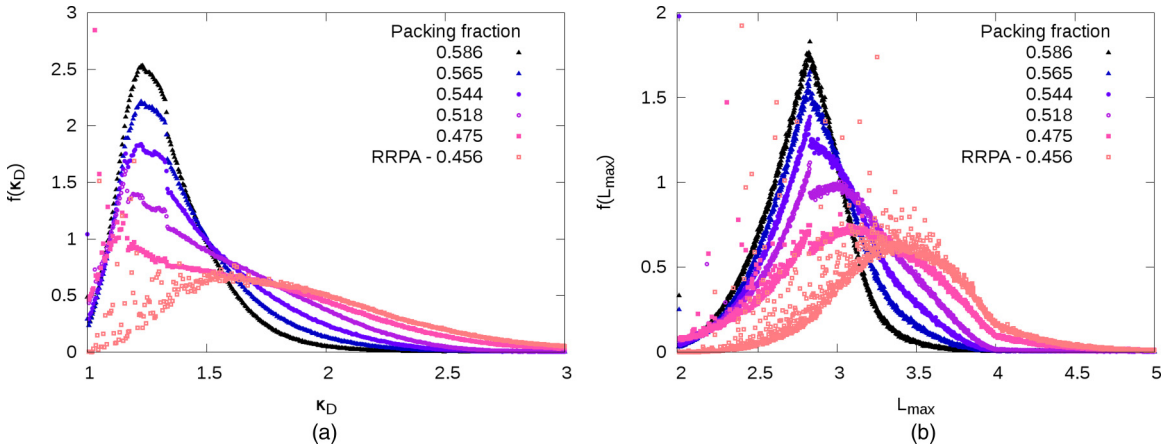

FIG. 5. Normalized distributions of (a) κ_D and (b) $L_{\max}$ for various packing fractions. Aggregates were generated with the MAX-1 algorithm, with the exception of the RRPA. Error bars are smaller than the point size.

fraction presents a much more homogeneous structure than the RRPA.

Figure 5(a) presents various distributions of κ_D obtained for aggregates built using the MAX-1 algorithm (RIPA) and one RRPA and Fig. 5(b) represents the distribution of $L_{\max}$ for the same aggregates. Concerning MAX-1, these distributions present very similar behaviors: Their maximum decreases with packing fraction while their full width at half maximum (FWHM) increases when packing fraction decreases. A bimodal component appears for the lowest-packing-fraction aggregates on both distributions, respectively centered around $\kappa_D \approx 2$ and $L_{\max} \approx 3.5$. These two values may be related in this way: Assuming that tetrahedra with $L_{\max} \approx 3.5$ have their five other edge lengths regularly distributed in the range [2,3.5] leads to a κ_D value of approximately 1.96, i.e., close to 2, suggesting that these two modes are indeed associated. The δ peaks appear for the lowest packing fraction, which is consistent with the existence of well defined distances observed on pair distribution functions for the same aggregates, noting the existence of regular polytetrahedra and recurrent configurations of spheres in the structure (see [9]). The RRPA, on the other hand, appears as a limiting case. Indeed, the first peak observed for κ_D and $L_{\max}$ distributions in the case of MAX aggregates completely disappears and is replaced by a series of δ peaks (some out of scale) and a slow evolution with respect to the second mode of the distributions of MAX aggregates.

Moreover, the distributions of κ_D present a discontinuity at $\kappa_D \approx 1.33$, and the distributions of $L_{\max}$ have one at $L_{\max} = 2.827$, which is likely associated with the former. The distributions of the lowest-packing-fraction aggregates have a change of slope for $L_{\max} = 4$. Additional work is needed to analyze precisely the configurations corresponding to these discontinuities.

C. Average values of distortion parameters

Although average distortion parameters are basic structural parameters, they do not determine the packing fraction of the aggregate because they only involve the short-range order of spheres (through the tetrahedral description) but do not take into account longer-range order. It is therefore worth studying the variation of packing fraction with distortion parameters for all aggregates. Overall, on average, the higher the packing fraction, the less distorted the tetrahedra, which can appear as slightly counterintuitive as the lowest-packing-fraction aggregates have a high RP component in their structure and as RP means a regular tetrahedral basis.

Figure 6(a) presents the dependence of $\bar{\kappa}_D$ on packing fraction, which decreases when γ increases and turns out to be linear for each family of algorithms. More specifically, the various algorithms are roughly distinguished as, for MAX-i aggregates, the average distortion increases with i for a given packing fraction. The RMIN-MAX-1 aggregate stands on its own, with a slightly different slope. The same is observed for RAN-i aggregates, which span a larger interval of $\bar{\kappa}_D$ for a given packing fraction (approximately 3 times as wide as that of MAX aggregates) and a certain overlap is observed as MAX-1 to MAX-4 are between RAN-4 and RAN-6 for $\gamma < 0.5$, which is the maximum packing fraction that RAN aggregates can reach.

The behavior of $\bar{L}_{\max} = f(\gamma)$ is globally the same [Fig. 6(b)] as it also decreases when packing fraction increases. However, its behavior deviates more from linearity: In the case of MAX-1 and RMIN-MAX-1 aggregates a change of slope is observed between 0.47 and 0.5 and they behave very differently from the rest of the aggregates, with a higher value of $\bar{L}_{\max}$ than any other aggregate for a given packing fraction. Furthermore, there is no overlap between RAN and MAX aggregates. The RAN aggregates appear more dispersed than MAX aggregates and, for the latter, they more or less converge on the same curve (that of MAX-9) with the noticeable exception of MAX-1 aggregates. Hence, surprisingly, the average distortions measured by both indicators do not agree as, for example, in the case of $\bar{\kappa}_D$, RMIN-MAX-1 aggregates appear as the least distorted and as the most distorted according to $\bar{L}_{\max}$.

D. Proportion of regular and quasiregular Delaunay tetrahedra

Using either distortion parameter, it is possible to evaluate the volume fraction of regular Delaunay tetrahedra (Φ_V, with $\kappa_D = 1$ or $L_{\max} = 2$), which globally decreases when the packing fraction increases, as the RP component of aggregates decreases also. The RRPA algorithms in particular give the highest Φ_V, ranging from 0.101 for $\gamma = 0.452$ to 0.073 for

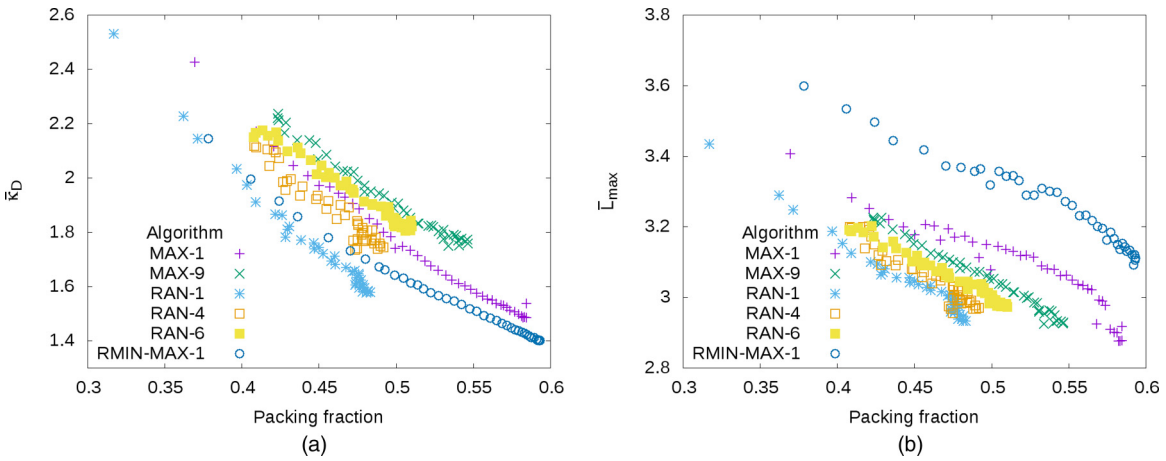

FIG. 6. Dependence of (a) $\bar{\kappa}_D$ and (b) $\bar{L}_{\max}$ with packing fraction. Error bars are smaller than the point size.

$\gamma = 0.415$. These values remain rather low and prompt the following question: What is the geometrical upper bound of the volume fraction of regular tetrahedra in random aggregates?

The results for random packings of RIPA type are presented in Fig. 7(a), which represents the variation of Φ_V with packing fraction. The highest proportion is obtained for RAN-6 aggregates ($\Phi_V = 0.141$ and $\gamma = 0.422$). RAN-1 turns out to be the family of aggregates with the smallest fraction of perfect tetrahedra for $\gamma \in [0.45,0.48]$; outside of this interval, it is RMIN-MAX-1. The proportion of perfect tetrahedra goes to 0 at the highest packing fractions.

Anikeenko and Medvedev [7] have studied the volume fraction of quasiregular Delaunay tetrahedra (PQRT), i.e., with $L_{\max} < 2.3$, within aggregates generated with JT and LS algorithms [see Fig. 7(b) of the present article]. They have found that this volume proportion increases with packing fraction in their studied interval of packing fraction, i.e., roughly between 0.53 and 0.71. Figure 7(b) superimposes their results with the ones found in the present study. Interestingly, the curves for MAX-4 and MAX-3 match over a rather narrow packing fraction interval, around $\gamma = 0.55$, and all MAX-i and RMIN-MAX aggregates show a similar increase of the volume fraction of tetrahedra with $L_{\max} < 2.3$ for $\gamma \in [0.56,0.59]$, however with less satisfying quantitative agreement. The highest value of the volume fraction of quasiregular tetrahedra found here is 0.127 and is obtained for RMIN-RRPA aggregates.

This comparison shows that regular and quasiregular tetrahedra are two distinct populations: Φ_V decreases when the packing fraction increases and goes to 0 beyond a threshold that depends on the algorithm but is roughly $\gamma = 0.57$, whereas PQRT goes to a minimum for a given packing fraction that depends on the algorithm (between $\gamma = 0.55$ and $\gamma = 0.57$) and then increases with packing fraction beyond this value of γ.

V. EFFECT OF SPHERE COORDINATION

The CCN of each sphere is determined when the aggregate is built: When a sphere is added in contact with another one, both their CCNs are increased by 1. Hence, by the end of the building process, each sphere is associated with its CCN.

A. Contact coordination number

1. *Partial distributions of contact coordination numbers*

Let η_{ij} be the number of contacts between spheres with CCNs i and j, respectively. The (normalized) distributions of η_{ij} can be easily determined from the sphere positions for all values of i and j. Figure 8 introduces distributions of η_{ij} for three aggregates built by RMIN-MAX-1 algorithms, from the highest to the lowest packing fraction [Figs. 8(a)–8(c)] and a RRPA [with the highest packing fraction among RRPAs; see Fig. 8(d)].

These distributions show a progressive shift of the maxima from high to low packing fraction [Figs. 8(a)–8(c)]. At high packing fraction, spheres with low CCN tend to be surrounded by spheres with higher CCN, thus reducing local fluctuations of the CCN. Then, as the packing fraction decreases, all η_{ij} curves more or less collapse, meaning that in this regime, all spheres, whatever their contact coordination number η_i, have the same η_{ij} distribution, centered on the average contact coordination number, hence a very similar environment in terms of contact neighbors. Finally, for even lower packing fraction, an inversion is observed and high-CCN spheres are preferentially surrounded by high-CCN spheres, which corresponds to a contact segregation effect. At the same time, the FWHMs of the distributions widen as the packing fraction decreases and they become less symmetrical. For the lowest packing fraction [Fig. 8(c)] η_{ij} distributions are very highly spread, with still a higher proportion of high-CCN spheres in the vicinity of other high-CCN spheres.

The RRPA presents rather similar η_{ij} distributions [Fig. 8(d)] as low-packing-fraction RIPAs, going through a minimum for η_{i5}. However, the order of the various η_{ij} distributions appears inverted in the case of the RRPA as, on the high-j end, the spheres with the highest proportion of contact with high-CCN spheres are spheres with lower CCN (i), i.e., $\eta_{3,11} > \eta_{4,11} > \cdots > \eta_{12,11}$, whereas for RIPA with low packing fraction, the opposite situation is observed, i.e., $\eta_{12,11} > \eta_{11,11} > \cdots > \eta_{3,11}$ [Fig. 8(c)].

2. *Evolution of $\langle \eta_{ij} \rangle$ around spheres with i*

The average value of η_{ij} around spheres with CCN i, $\langle \eta_{ij} \rangle$, can easily be determined from the distributions

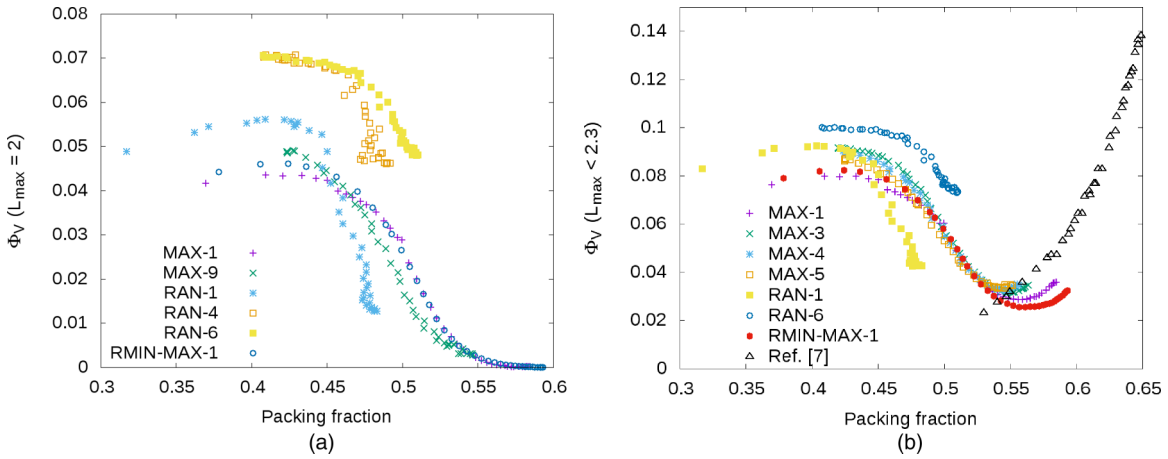

FIG. 7. (a) Dependence of the volume fraction Φ_V of perfect tetrahedra ($L_{\max} = 2$) with packing fraction. (b) Dependence of the volume fraction Φ_V of tetrahedra with $L_{\max} < 2.3$ for the aggregates of the present study and results obtained by Anikeenko and Medvedev in [7].

presented above. Figure 9 presents the evolution of $\langle \eta_{ij} \rangle$ for all values of i as a function of packing fraction for MAX-1 and RMIN-MAX-1 algorithms. The inversion suggested by the shift of the maximum of distributions in the preceding section appears clearly for RMIN-MAX-1 aggregates [Fig. 9(b)] as they form a crossover for $\gamma \approx 0.52$ which separates a low- and a high-packing-fraction regime. In the low-packing-fraction regime, high-coordination spheres tend to be surrounded by spheres with higher CCN than the spheres surrounding low-CCN sphere, i.e., $\langle \eta_{12,j} \rangle > \langle \eta_{11,j} \rangle > \cdots > \langle \eta_{4,j} \rangle$, with the exception of the limit case $\langle \eta_{3,j} \rangle$, corresponding to the segregation effect seen when discussing η_{ij} distributions. In the high-packing-fraction regime, this situation is inverted: Spheres with low CCN are surrounded,

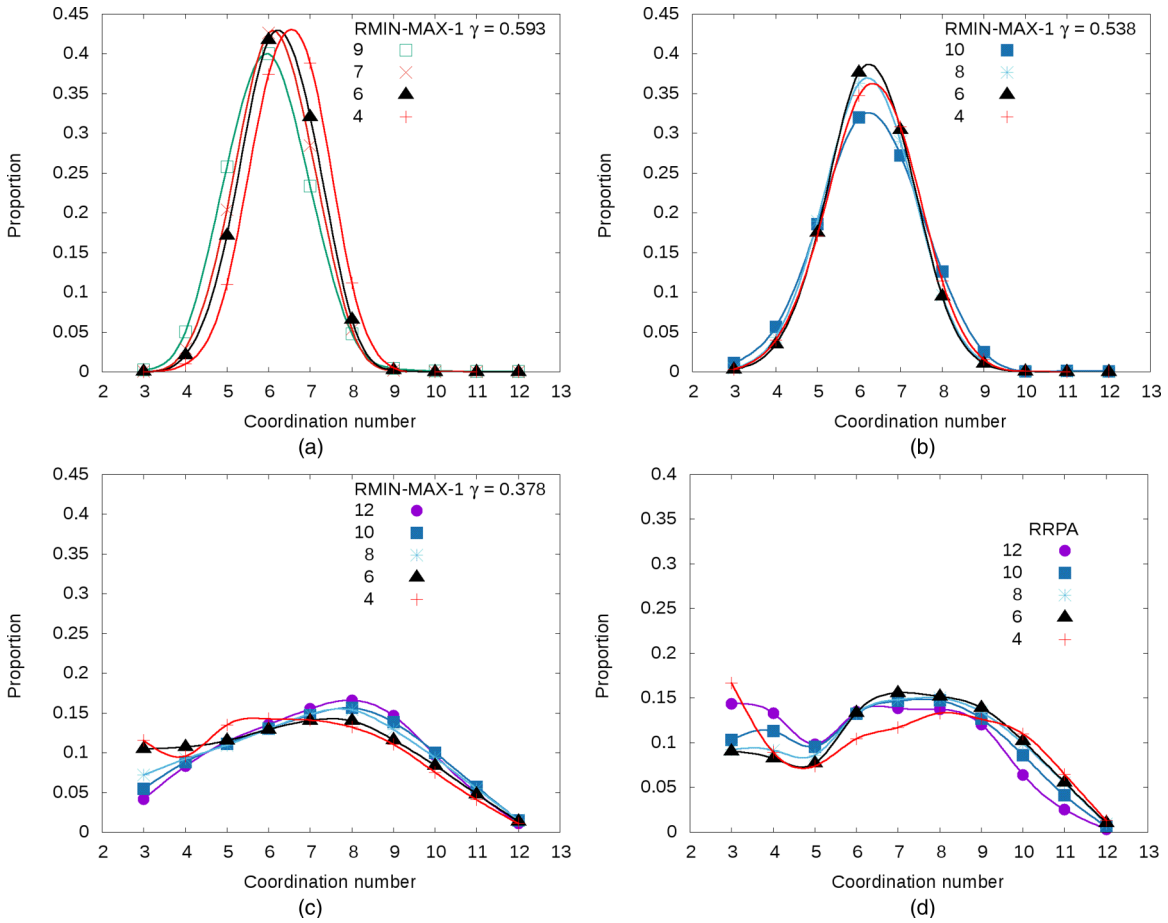

FIG. 8. Normalized distributions of η_{ij} (lines are mere guides for the eye) for aggregates produced by the RMIN-MAX-1 algorithm with (a) $\gamma = 0.593$, (b) $\gamma = 0.538$, and (c) $\gamma = 0.378$ and for (d) the RRPA with $\gamma = 0.456$.

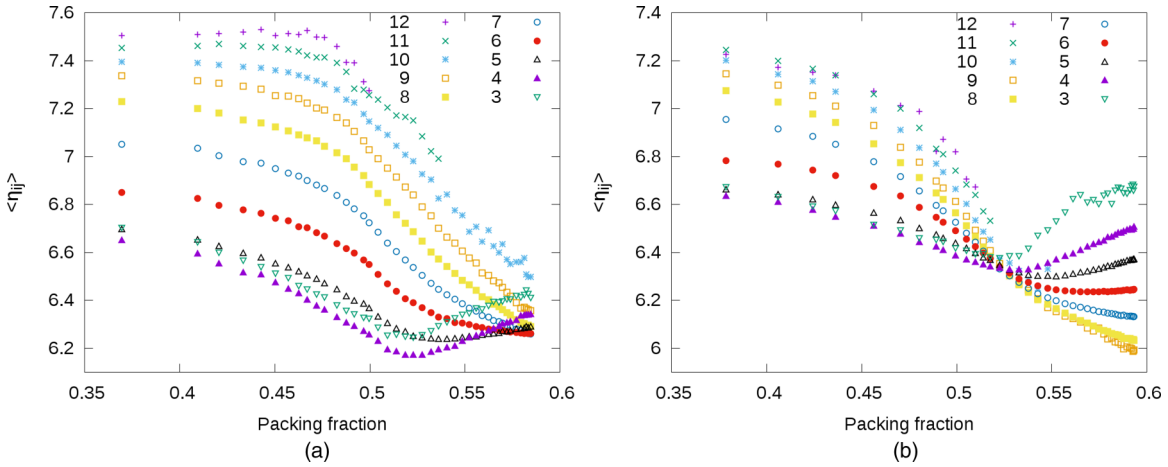

FIG. 9. The $\langle \eta_{ij} \rangle$ for various values of i in the case of the (a) MAX-1 and (b) RMIN-MAX-1 algorithms.

on average, by spheres with higher CCN, thus reducing density fluctuations.

In the case of aggregates generated by the MAX-1 algorithm, this crossover is not captured but might take place at higher values of packing fraction (unaccessible by this algorithm) as all curves begin to collapse for $\gamma > 0.55$. In this case, only the low-packing-fraction regime is observed.

3. *Radial dependence of the average contact coordination number*

The radial dependence of the average contact coordination number $\langle \mathrm{CCN} \rangle$ of spheres within $[r, r+dr]$ from an i coordinated sphere has been determined for all aggregates and all values of i. Figure 10 introduces two examples obtained for the RMIN-MAX-1 aggregates with the highest and lowest packing fractions [Figs. 10(a) and 10(b)].

At high packing fraction [see Fig. 10(a)], the average value of the CCN of spheres at a distance $r < 3.5$ from a low coordinated sphere is higher than that of spheres surrounding a sphere with higher CCN. Then, as the packing fraction decreases, the relative positions of the various curves for $r < 3.5$ are progressively inverted: They are superimposed for $\gamma \approx 0.54$, which incidentally matches the packing fraction of the crossover of the various $\langle \eta_{ij} \rangle$ curves in Fig. 9(b) for the same aggregates. At even lower packing fraction, the inversion is complete as it is exemplified in Fig. 10(b): Low coordinated spheres are on average surrounded by quasi-first-neighbor spheres with low CCN and vice versa. This regime corresponds to a segregation effect in the range of quasifirst neighbors instead of contact neighbors. At even larger values of r ($r > 4$), this segregation effect gets inverted.

All curves end up superimposed on one another beyond some value $r = r_e$, however r_e increases when the packing fraction decreases (from $r_e \approx 4$ for $\gamma = 0.593$ up to $r_e \approx 6.5$ for $\gamma = 0.378$), suggesting that structural inhomogeneities extend over larger and larger scales as γ decreases. Discontinuities are observed at $r = d\sqrt{3}$ and $r = 2d$, which match discontinuities of the various pair distribution functions (PDFs) of the same aggregates (cf. Sec. V C 1 b below and [9]). The amplitude of these discontinuities increases with the CCN of the central sphere. At low packing fraction [Fig. 9(b)], strong local increases of $\langle \mathrm{CCN} \rangle$ are noticeable for values of r which match δ peaks on the PDF, hence corresponding to distances characteristic of the presence of regular polytetrahedra in the aggregate (cf. Sec. V C 1 b below).

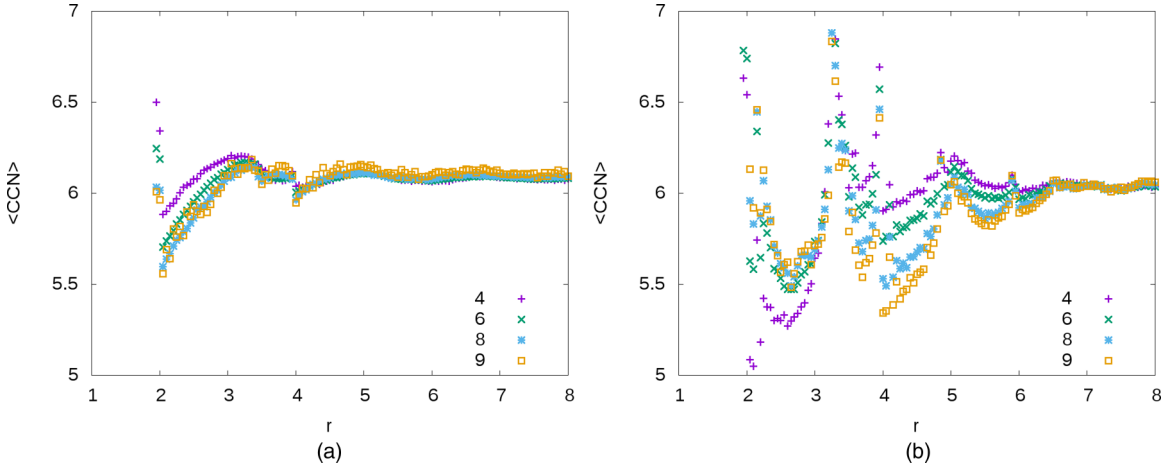

FIG. 10. Radial value of the average CCN around i coordinated spheres in RMIN-MAX-1 aggregates with (a) $\gamma = 0.593$ and (b) $\gamma = 0.378$.

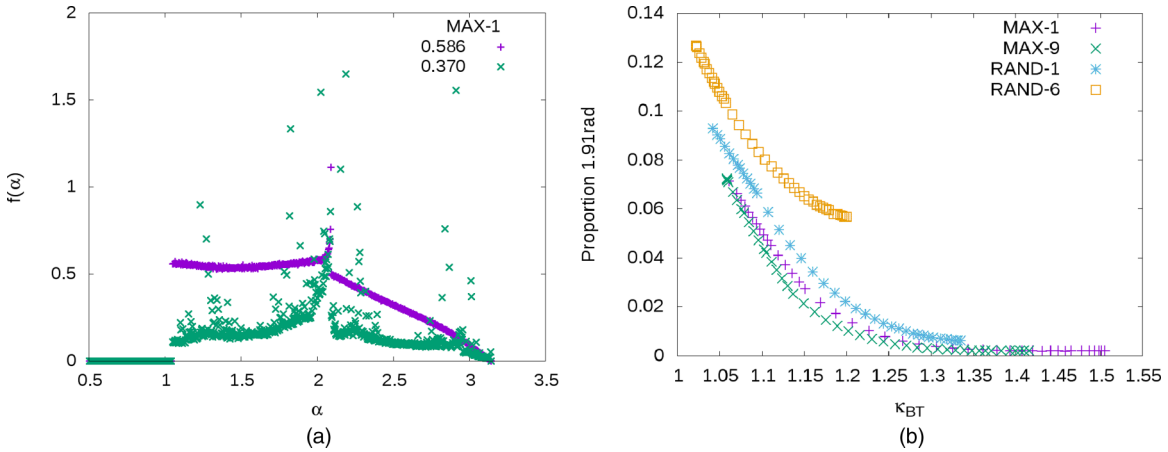

FIG. 11. (a) Bond angle distributions for high- and low-density aggregates (values for $\alpha = \pi/3$ fall out of the range of the figure). (b) Dependence of the 1.9106-rad δ peak in the bond angle distribution with the irregularity index of building tetrahedra $\bar{\kappa}_{\mathrm{BT}}$.

B. Bond angle distributions

Two spheres i and j form a bond when they are contact neighbors. The bond angles α around a sphere i are defined as the angles formed between all possible vectors $\vec{R}_{ij}$ between contacting neighbors. Hence, for a sphere i with n contact neighbors there are $n(n-1)/2$ bond angles.

1. Global bond angle distributions

Bond angle distributions α have been calculated. The smallest possible bond angle is between three contacting spheres, i.e., $\alpha = \pi/3$, and the largest is of course π.

Figure 11(a) presents bond angle distributions for the most and least dense aggregates obtained by the MAX-1 algorithm. It shows that the distribution of the densest aggregate is mostly smooth, marked by two discontinuities. The first one, the minimum value, is $\alpha = \pi/3$, which corresponds to the configuration of three spheres in contact with each other. The value here is so high that it is outside the scale of the figure. The second discontinuity occurs for $\alpha = 2.093 \pm 0.002$, close to $2\pi/3$, which corresponds to the situation where four spheres form two coplanar equilateral triangles sharing a common side. In [19] Karayiannis *et al.* obtained a very similar bond distribution in their structures of chains of joined monodisperse hard spheres in the maximally random jammed state. The main difference is the broader shape of the peaks in the distributions of Ref. [19], which we interpret as a finite-size broadening since the maximum number of spheres considered in [19] is 54 000 instead of the 10^6 used here.

For the aggregate with the smallest density, many singularities appear, in the same way as δ peaks appear on its pair distribution function. On the PDF, these δ peaks are characteristic of the presence of regular polytetrahedra in the disordered structure (see [9]). The addition of another sphere on top of three contacting ones does not introduce a new bond angle. The addition of a fifth sphere then forms a trigonal bipyramid, with $\alpha \approx 1.9106$ rad. This angle should correlate with the δ peak at $r = d\sqrt{8/3}$ observed on the pair distribution function of low-density aggregates (see [9]). It shows the same smooth dependence with the irregularity index of building tetrahedra [see Fig. 11(b)] as $P(r = d\sqrt{8/3})$.

2. Partial bond angle distributions

Bond angle distributions for specific contact coordination numbers are shown in Fig. 12. Their global behavior is similar to global bond angle distributions, but peculiarities can be seen, in the function of packing fraction and/or contact coordination number.

It turns out that for aggregates with high packing fraction, the angular environment depends strongly on the CCN. Low-CCN spheres have a stronger asymmetry between $\alpha = \pi/3$ and $\alpha = 2\pi/3$ than spheres with high CCN. For high-packing-fraction aggregates, the distribution of low-CCN spheres shows a depletion of lower bond angles and an excess of high angles and the distribution becomes more even when the CCN increases. When the packing fraction decreases, low- and high-CCN spheres tend to have more similar angular environments.

The appearance of regular polytetrahedra, associated with δ peaks, like in the case of the global bond angle distribution, is logically correlated with a decrease of the continuum component of the distribution. This continuum disappears completely for the RRPA [Fig. 12(d)].

C. Partial pair distribution functions

The structure of random sphere packings is usually characterized by the probability per unit volume of finding a sphere center at a distance r from another sphere center $P(r) \times N/V$, where N is the number of spheres in the aggregate of volume V and the PDF $P(r)$ is normalized to 1 when $r \to \infty$.

Distinguishing spheres by their contact coordination number allows a much more detailed structural description by partial pair distribution functions (PPDFs), which are defined as the probability $P_{ij}(r)$ of finding a sphere with contact coordination number j at a distance r from another sphere with contact coordination number i, normalized to 1 at large r.

1. Principle for partial PDFs $P_{ii}(r)$, $P_{ij}(r)$, and $P_i(r)$

In practice, coordination numbers range from 3 to 12, the maximum CCN in three-dimensional space. For a spherical

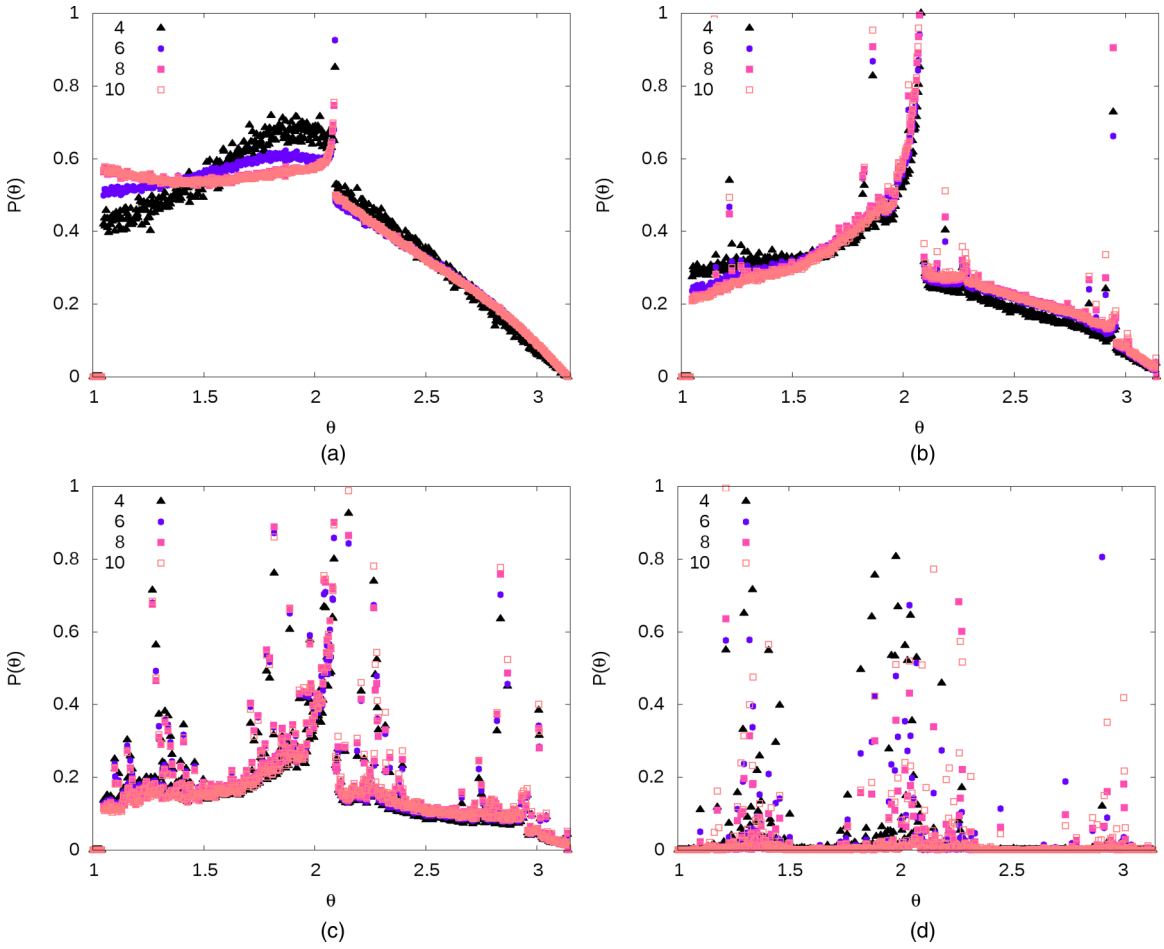

FIG. 12. Partial bond angle distributions for various MAX-1 aggregates with (a) $\gamma = 0.586$, (b) $\gamma = 0.500$, and (c) $\gamma = 0.370$, and (d) one RRPA with $\gamma = 0.456$. Values for $\alpha = \pi/3$ fall out of the range of the figure.

aggregate with radius R, $P_{ij}(r)$ is written

$$P_{ij}(r) = \frac{V^2}{N_i N_j} \frac{\Delta N_{ij}}{(2-\delta_{ij}) S(r) \Delta r}, \tag{7}$$

where N_i and N_j are the numbers of spheres with CCNs i and j, respectively, in the volume $V = 4\pi R^3/3$ of the aggregate; ΔN_{ij} is the number of sphere pairs of CCNs i and j, respectively, lying in the interval $[r, r + \Delta r]$; δ_{ij} is the usual Kronecker symbol; and $S(r)$ is the spherical shape factor of the aggregate [20]

$$S(r) = \frac{\pi^2}{6} r^2 (2R - r)^2 (4R + r). \tag{8}$$

The $P_{ii}(r)$ PPDFs describe the arrangement of i coordinated spheres, while the $P_{ij}(r)$ PPDFs with $i \neq j$ describe the mutual arrangement or chemical order between i and j coordinated spheres. In the case of sticky hard spheres with diameter d, the peak of contacting neighbors in $P_{ij}(r)$ is represented by [21]

$$P_{ij}(d) = \bar{\eta}_{ij} \frac{V}{4\pi N_j d^2} \delta(r - d), \tag{9}$$

i.e., numerically, $\bar{\eta}_{ij} = 3 \frac{N_j}{R^2} d^2 2\sigma P(d)$, where $\bar{\eta}_{ij}$ is the average number of j coordinated spheres contacting an i coordinated sphere and $\sigma = 0.01$ is the length step used in $P(r)$ calculations. Numerical values of $P_{ij}(d)$ fall out of range of the $P_{ij}(r)$ figures presented below.

One can then define the probability $P_i(r)$ to find a sphere with any coordination number at a distance r from a sphere with coordination number i. It is written

$$P_i(r) = \sum_{j=3}^{12} C_j P_{ij}(r), \tag{10}$$

where $C_j = N_j/N$ is the concentration of j coordinated spheres ($N = \sum_{j=3}^{12} N_j$). These $P_i(r)$ characterize the global arrangement of spheres around a sphere with coordination number i. Finally, the global PDF is written

$$P(r) = \sum_{i=3}^{12} C_i P_i(r). \tag{11}$$

a. Random regular polytetrahedral aggregates. Figure 13 presents $P_{ii}(r)$ curves (with $i = 4$, 6, and 8) of a RRPA with $\gamma = 0.418$, as well as its global PDF (see [9] for the calculation procedure of the latter). Concerning the global PDF, a striking difference from what was observed for the RIPA (see [9]) is the disappearance of the topological discontinuities at $r = \sqrt{3}d$ and $r = 2d$. The continuous structure of the PDF observed in RIPAs almost disappears and is replaced by a set of polyhedral

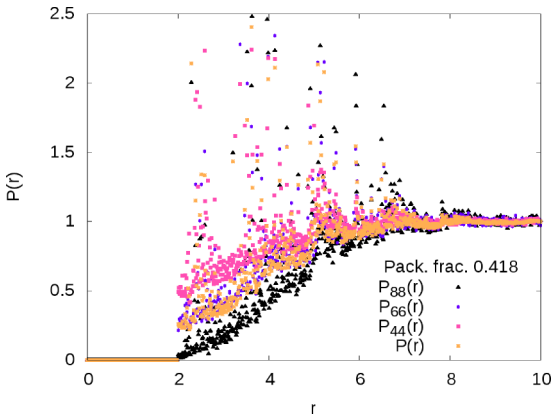

FIG. 13. Global and partial pair distribution functions [$P(r)$ and $P_{ii}(r)$ for $i = 4$, 6, and 8] for a random regular polytetrahedral aggregate.

δ peaks ([11,21]), which are due to a large (virtually infinite) regular polytetrahedron. The positions of these peaks, which are due to precise configurations of spheres with well defined distances, are identical to those studied by Medvedev and Pilyugina [11]. The continuous structure grows almost linearly as a function of r and goes to 1 for $r \approx 3.5d = 7$.

The partial PDFs $P_{ii}(r)$ show a systematic tendency, as their continuous regime in the region of the quasifirst neighbors (QFNs) starts from 0 for spheres with coordination number i equal or superior to 8 and increases like the global $P(r)$. The lower coordination numbers ($i < 8$) lead to $P_{ii}(r)$ starting from higher values in the QFN area. This can be qualitatively understood: The more contacting first neighbors a sphere has, the fewer quasifirst neighbors it can accept.

b. Random irregular polytetrahedral aggregates. The global PDF of RIPAs was studied in [9], with the exception of RMIN aggregates. However, the latter introduce no qualitative differences to these results.

The PPDFs $P_{ii}(r)$ together with the corresponding PDF are presented in Figs. 14(a) and 14(b) for MAX-1 aggregates with the two most extreme packing fractions $\gamma = 0.586$ and $\gamma = 0.370$. First and foremost, for a given packing fraction, the number of quasifirst neighbors (corresponding to values of r close to d) decreases when the coordination number (i) increases, like in the case of RRPAs and for the same reasons: The more contacting neighbors a sphere has, the fewer quasifirst neighbors it can accept.

On the other hand, the comparison between Figs. 14(a) and 14(b) shows that the number of quasifirst neighbors decreases with packing fraction. At low packing fractions, they form plateaus whose level increases when the coordination number decreases, whereas they have a very distinct behavior for high packing fractions: Low coordination number spheres possess many quasifirst neighbors, while high coordination number spheres have a very limited number of QFNs. Both topological discontinuities (at $r = \sqrt{3}d$ and $r = 2d$) increase when the coordination number increases and when packing fraction increases.

Finally (see the Appendix for figures), isopacking-fraction and iso-$\bar{\kappa}_D$ aggregates obtained by different building algorithms show significant differences in their global and partial PDFs, confirming that parameter γ and $\bar{\kappa}_D$ are insufficient for a full structural description of random aggregates. Aggregates sharing similar values of these two parameters (γ and $\bar{\kappa}_D$) still present significant differences in structural properties. Hence, even when used together, γ and $\bar{\kappa}_D$ are not satisfying predictors of structural properties of disordered systems. Besides, it has been impossible to find aggregates with similar $\bar{L}_{\max}$ and γ to compare them in a similar fashion, leaving the question open for a possible combination of these two parameters as a good predictor of the global structure of random aggregates. Conversely, it turns out that PPDFs allow a more sensitive distinction between aggregates built by different algorithms than the corresponding global PDF and are thus interesting structural descriptors.

A sampling of $P_{ij}(r)$ (with $i \neq j$) curves is shown in the Appendix. They show that QFNs are favored by higher packing fractions and lower coordination numbers i and j. The implicit chemical ordering in these curves will be studied in more detail hereafter.

The $P_i(r)$ (for $i = 4$, 6, and 9) obtained for aggregates built by the MAX-1 algorithm with packing fractions 0.370 and 0.586 are displayed in Fig. 15. These PPDFs appear to depend strongly on i and the packing fraction. On the one hand, for each packing fraction (a) quasifirst neighbors

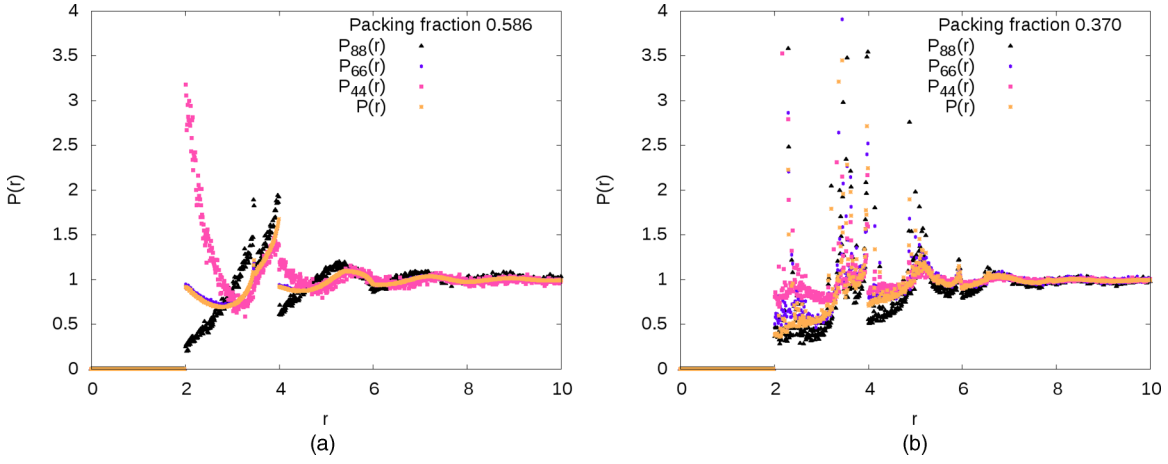

FIG. 14. Samples $P(r)$ and $P_{ii}(r)$ obtained for aggregates generated by the algorithms (a) MAX-1 ($\gamma = 0.586$) and (b) MAX-1 ($\gamma = 0.370$).

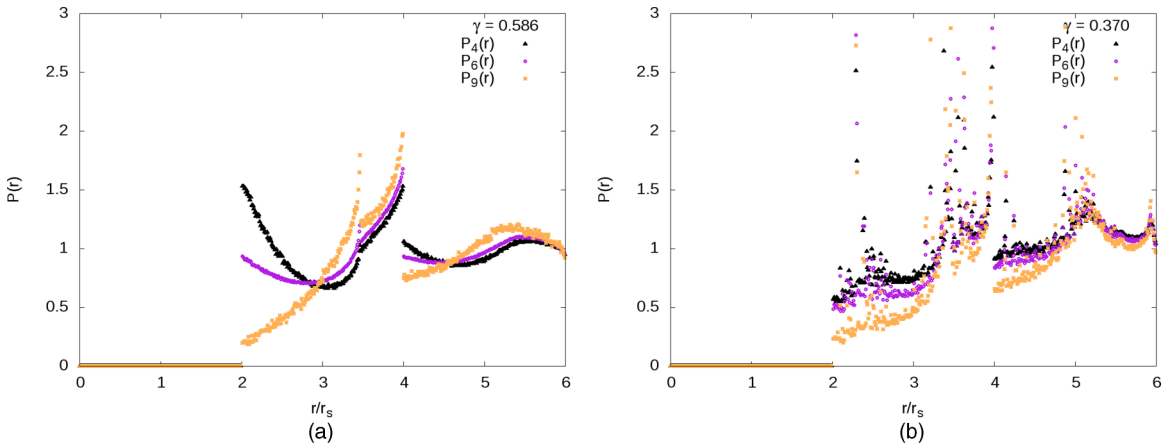

FIG. 15. The $P_i(r)$ for two packing fractions generated by the algorithm MAX-1.

increase when the coordination number decreases and (b) topological peaks at $r = d\sqrt{3}$ and $2d$ are more intense for high coordination numbers. On the other hand, the main differences between low- and high-packing-fraction aggregates are that (i) polytetrahedral δ peaks are noticeable on aggregates with low packing fractions, (ii) the transition from the high to the low packing fraction is mostly due to a decrease of quasifirst neighbors around low coordination spheres, and (iii) in the case of the densest aggregate, P_i oscillations are increasingly shifted toward smaller-r values as the coordination number i increases, while such a shift is not observed for the lowest-packing-fraction aggregate.

D. Radial evolution of local packing fraction from pair distribution functions

1. Principle

Knowing pair distribution functions, it becomes possible to study the variation of the local packing fraction around an average sphere as a function of r. Using the relation (3), the packing fraction of a sphere $\mathcal{S}$ with arbitrary diameter $R_{SC} > d$ situated within the aggregate is written

$$\gamma(R_{SC}) = \frac{4\pi r_s^3/3 + \rho \int_0^{R_{SC}+r_s} P(r) 4\pi r^2 V_s(r, R_{SC}) dr}{4\pi R_{SC}^3/3}, \tag{12}$$

with $\rho = N/V$ the number of spheres per unit volume in the aggregate. The $4\pi r_s^3/3$ term corresponds to the sphere in $r = 0$, $V_s(r)$ is defined by Eq. (3), and $P(r)$ can be a total or partial pair distribution function. In addition, $\gamma(r \leqslant r_s) = 1$.

It is also possible to remove the contribution of the central sphere and its contact first neighbors to the packing fraction, which is written

$$\gamma_{CN}(R_{SC}) = \frac{4\pi r_s^3/3 + i V_s(r = d, R_{SC})}{4\pi R_{SC}^3/3}, \tag{13}$$

where i is the number of contacting neighbors of the central sphere. We then have

$$\gamma_{WCN}(R_{SC}) = \gamma(R_{SC}) - \gamma_{CN}(R_{SC}), \tag{14}$$

where γ_{WCN} is the contribution to the packing fraction of the quasifirst and further neighbors around an average sphere.

2. Local packing fraction around an average sphere

Using the global PDF, the formalism just introduced gives access to the variation of the local packing fraction as a function of r around an average sphere. Figure 16(a) represents $\gamma(R_{SC})$ and Fig. 16(b) represents $\gamma(R_{SC})/\gamma$, which goes to 1 as R_{SC} goes to ∞. All aggregates behave differently depending on their packing fraction. For the densest ones, the packing fraction falls below the average value, before converging more rapidly at large r than the least dense ones. On the other hand, in the case of the least dense ones, the packing fraction remains above the average value and converges more slowly. Oscillations of local packing fractions are damped at about $r = 5d$ for the lowest packing fraction and around $r = 3d$ for the highest packing fraction.

3. Local packing fraction around i coordinated spheres

Using $P_i(r)$, it is possible to determine the local packing fraction as a function of r for an average sphere with coordination number i, γ_i. Figures 16(c) and 16(d) present the sets of corresponding curves for the two MAX-1 aggregates with the lowest and highest packing fractions. The short-range local density grows with the coordination number and the packing fraction of the aggregate. Significant oscillations are observed for the aggregate with the highest packing fraction. Their amplitude is damped for the aggregate with the lowest packing fraction. Figures 16(e) and 16(f) show the evolution of the packing fraction without the contribution of contact neighbors (γ_{WCN}) and the central sphere, hence only that of the quasifirst and further neighbors. As it could be expected, the lower number of QFNs around spheres with high coordination numbers leads to a significantly lower packing fraction due to QFNs than in the case of spheres with low contact coordination number.

In the case of the aggregate with the highest packing fraction [Fig. 16(e)], the various curves converge for $R_{SC} \approx 3.5d$ and the highest difference is observed between $i = 10$ and $i = 3$ for $R_{SC} \approx 2.53$, $\gamma_{WCN,3} - \gamma_{WCN,10} \approx 0.28 = 0.48\gamma_{ag}$. Between $i = 10$ and $i = 6$, the maximum is found at $R_{SC} \approx 2.57$, with $\gamma_{WCN,6} - \gamma_{WCN,10} \approx 0.16 = 0.27\gamma_{ag}$.

There is a much lower difference in contribution of the QFN between spheres with different contact coordination number

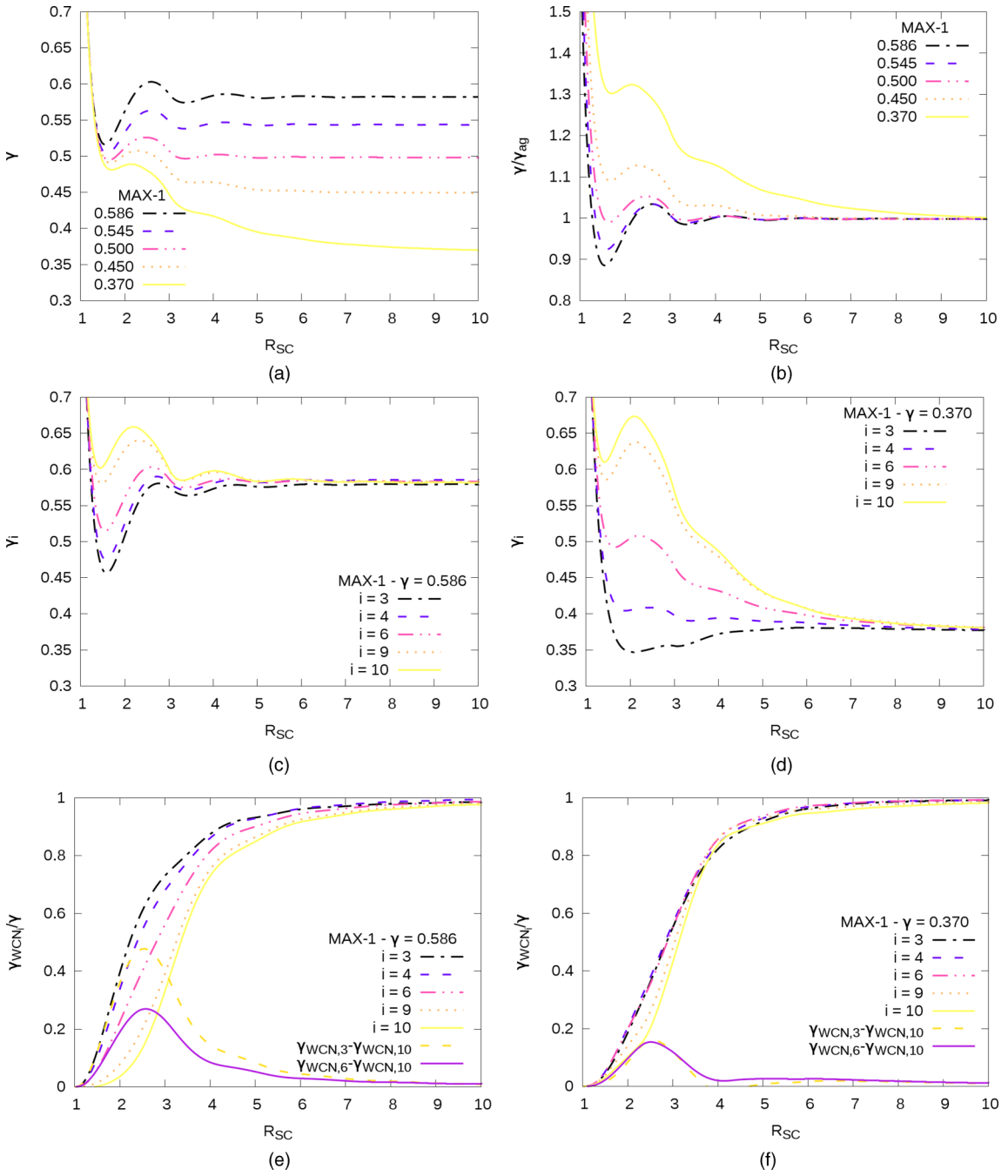

FIG. 16. (a) Local packing fraction and (b) local packing fraction divided by the average packing fraction for various MAX-1 aggregates. The radial evolution of the packing fraction around i coordinated spheres is shown for MAX-1 aggregates with (c) $\gamma = 0.586$ and (d) $\gamma = 0.370$. Also shown is the radial evolution of the packing fraction around i coordinated spheres without contact neighbors [the relation (14)] for MAX-1 aggregates with (e) $\gamma = 0.586$ [the bottom lines represent the difference between the highest and lowest bound, i.e., $\gamma_{\mathrm{WCN},3}(R_{\mathrm{SC}}) - \gamma_{\mathrm{WCN},10}(R_{\mathrm{SC}})$, and intermediate, i.e., $\gamma_{\mathrm{WCN},6}(R_{\mathrm{SC}}) - \gamma_{\mathrm{WCN},10}(R_{\mathrm{SC}})$] and (f) $\gamma = 0.370$.

in the case of the aggregate with the lowest packing fraction (in terms of absolute as well as relative value). However, the maximum of the difference between $\gamma_{\mathrm{WCN},3}$ and $\gamma_{\mathrm{WCN},10}$ is obtained for approximately the same value $R_{\mathrm{SC}} \approx 2.55$ and $\gamma_{\mathrm{WCN},3} - \gamma_{\mathrm{WCN},10} \approx 0.06 = 0.16\gamma_{\mathrm{ag}}$. Between $i = 10$ and $i = 6$, the maximum is found at $R_{\mathrm{SC}} \approx 2.51$, with $\gamma_{\mathrm{WCN},6} - \gamma_{\mathrm{WCN},10} \approx 0.06 = 0.16\gamma_{\mathrm{ag}}$, which is remarkably similar to the former. In this case, Fig. 16(e) shows that $\gamma_{\mathrm{WCN}}(R_{\mathrm{SC}})$ for coordination numbers below 7 behave very similarly, suggesting that these types of spheres have more or less the same environment in terms of number of QFNs, irrespective of their contact coordination number.

E. Global and partial structure factors

The previous structural description achieved by the PPDF analysis of random packings leads naturally to the study of the corresponding global and partial structure factors which

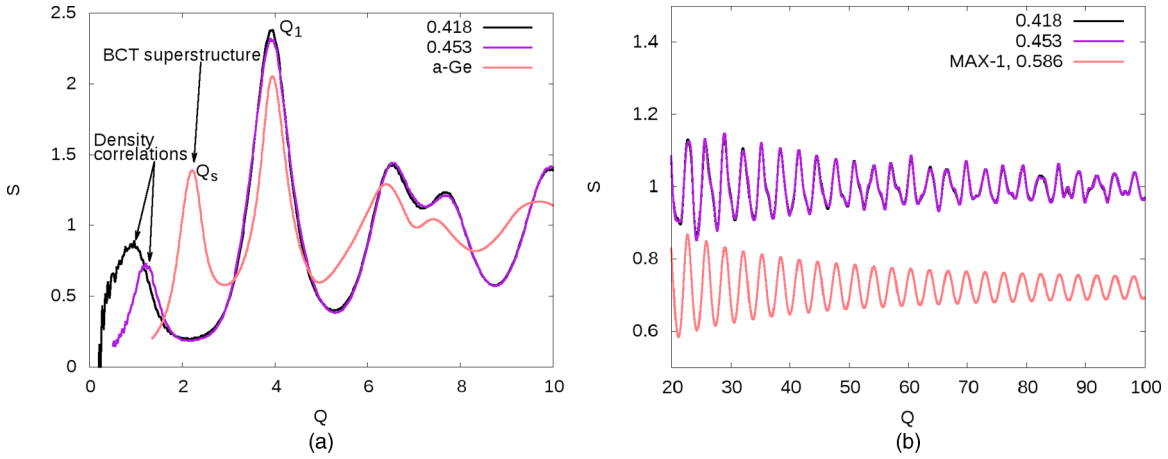

FIG. 17. (a) Structure factor of two RRPAs and experimental results obtained on amorphous Ge (a-Ge) (data obtained in [23]) at small Q and (b) large-Q behavior of the structure factor of the RRPAs and one (high-packing-fraction) RA.

can be compared with the results of diffraction experiments on disordered materials.

1. Global and Ashcroft-Langreth partial structure factors

Let us first introduce the global structure factor

$$S(Q) = 1 + \frac{N}{V}\int_0^\infty [P(r) - 1]\frac{\sin(Qr)}{Qr} 4\pi r^2 dr \qquad (15)$$

and the partial Ashcroft-Langreth (AL) structure factors, defined by

$$S_{ij}(Q) = \delta_{ij} + \frac{\sqrt{N_i N_j}}{V}\int_0^\infty [P_{ij}(r) - 1]\frac{\sin(Qr)}{Qr} 4\pi r^2 dr, \qquad (16)$$

where δ_{ij} is the Kronecker symbol. The diagonal terms S_{ii} represent the structure factors of the partial aggregates formed by spheres with contact coordination number i and will be studied first. The nondiagonal terms S_{ij} with $i \neq j$ describe the mutual or chemical arrangement between i and j coordinated spheres and will be studied later by the more suited Bhatia-Thornton formalism.

The $S(Q)$ and $S_{ij}(Q)$ values for $Q \ll 1/R$ cannot be calculated from the relations (15) and (16) owing to the finite radius R of the aggregates [9]. However, $S(Q = 0)$ values are determined by the statistical density fluctuations according to the relation [22]

$$S_{ij}(0) = \frac{\overline{N_i N_j} - \overline{N_i}\,\overline{N_j}}{\sqrt{\overline{N_i}\,\overline{N_j}}}, \qquad (17)$$

where overbars represent averages.

Fluctuations were directly derived from the positions of the sphere centers. To that purpose, a large cube with edge $50d$ centered on the aggregates origin was subdivided into 1000 subcubes with edge $5d$, each of them containing N_i and N_j sphere centers with respective coordination numbers i and j. Average values of $\overline{N_i}$, $\overline{N_j}$, and $\overline{N_i N_j}$ were taken over the 1000 subcubes to get the statistical fluctuations involved in the relation (17).

a. Random regular polytetrahedral packing–global structure factor. Figure 17 introduces the global structure factor of two RRPAs: small Q [Fig. 17(a)] and large Q or the asymptotic regime [Fig. 17(b)]. It turns out that the structure factors of the RRPA exhibit a prepeak, whose position depends on the algorithm or packing fraction used. The position and intensity of this prepeak corresponds to the folding of the polytetrahedra which controls the space correlation of density fluctuations. It accounts for interferences between high-density and low-density zones of the single polytetrahedron. At high Q, $S(Q)$ appears aperiodic due to the infinite series of $\delta(r_p)$ peaks in $P(r)$ corresponding to the distances between vertices in the infinite RRPA and is only weakly affected by small changes in packing fraction (depending on the algorithm used).

Comparison with the structure of tetravalent elements. The polytetrahedral structure factor can be usefully compared with the experimentally measured structure factors of pure tetravalent elements (C [24], Ge [23], and Si [25]) or with the tetrahedral structure of oxygen atoms in glassy water [26,27]. As a matter of fact, the structure of these elements is based on body-centered regular tetrahedra (BCT) connected by their vertices [28], while RRPAs are made from simple regular tetrahedra connected by their faces. As a consequence, a pseudosuperstructure peak for such hard-sphere-based centered tetrahedra should correspond to $Q_s/Q_1 = d_1/d_s = \sqrt{6}/4 = 0.612$, where d_1 is the distance between contacting atoms and d_s is the edge length of the regular centered tetrahedron. Experimentally, Etherington found $Q_s/Q_1 = 0.572$ [23] for the structure factor of amorphous Ge, Laaziri *et al.* found 0.583 for the same ratio in amorphous silicon [25], and Gaskell *et al.* found 0.540 for amorphous carbon [24]. The discrepancy from 0.612 for these three values could be due to the error introduced by the hard-sphere approximation of the tetrahedral bond angle between first neighbors of softer potentials, which does not allow reproducing perfectly the behavior of covalent materials.

However, this superstructure peak is lacking from the structure factor of RRPAs, but another small-angle peak at significantly lower value is found around $Q_s/Q_1 \approx 0.25$, varying with the packing fraction. The latter can be attributed to the pseudoperiodic correlation of density fluctuations present in the RRPA model. These correlations happen over larger distances than those of the BCT, hence the smaller-Q values of the corresponding prepeak. It corresponds roughly

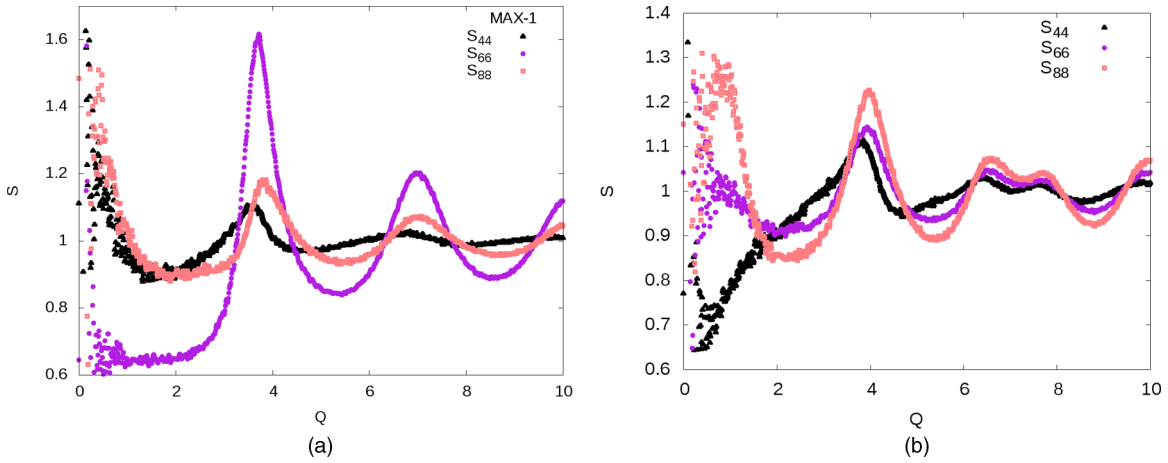

FIG. 18. Ashcroft-Langreth partial structure factor for (a) highest-packing-fraction RIPAs and (b) RRPAs.

to the end of significant oscillations of pair distribution functions.

The reason why this longer correlation-distance prepeak does not appear for tetravalent elements probably has to do with the fact that tetrahedra forming their structures are connected by vertices, allowing for many more degrees of freedom and preventing longer distances correlations than in the case of RRPAs where tetrahedra are connected by their faces, which is geometrically more constraining. On the other hand, the second peak of the structure factor of the RRPA splits into two subpeaks in a manner completely analogous to what is found in amorphous tetravalent elements.

Finally, for RRPAs, characteristic distances are strictly defined, giving rise to δ peaks on the PDF resulting in aperiodic large-Q behavior, also absent from the structure factor of tetravalent elements. In contrast, the lack of such well defined distances, because of higher degrees of freedom in the orientations of tetrahedra relative to one another in the case of tetravalent element, results in a single δ peak on their PDF, which accounts for their periodic behavior in the large-Q regime [21].

b. Random irregular polytetrahedral aggregates. The AL partial structure factors of random irregular polytetrahedral aggregates are presented in Figs. 18(a)–18(c), along with the partial structure factors of the RRPA [Fig. 18(d)]. These structure factors all have in common that the global amplitude of their oscillations increases from $i = 3$ up to $i = 6$ and then decreases as i increases beyond 6. Moreover, the position of the first peak of S_{ii} goes to small Q when the packing fraction increases (whatever i and γ). At large Q, there is no phase shift, whatever i and γ, and S_{ii} oscillates like $\sin(Qd)/Qd$ (not shown here).

Some peculiarities are also observed. A shoulder appears on the left of the first peak of S_{44} (around $Q = 3.8$). For S_{88} and S_{44} an intense prepeak around $Q = 0.8$ is noted, whose intensity increases with the packing fraction for S_{44} and decreases when the packing fraction increases for S_{88}. This prepeak is due to correlated density fluctuations between low- or high-density regions separated by an average distance of $2\pi/0.8r_s \approx 8r_s$ lying beyond the main P_{ii} oscillations; they are observed whatever the packing fraction, even if there is no noticeable prepeak on the global structure factor. In the case of S_{66}, $S_{66}(0)$ decreases when γ increases and barely any prepeak may be observed at all. The first peak remains symmetrical; its position depends little on the packing fraction. The first peak of S_{88} becomes strongly asymmetrical for the highest packing fraction.

Finally, a splitting of the second peak is observed on the AL structure factors with high coordination numbers and low packing fraction. This splitting was noticed above for the RRPA and it is consistent with the existence of a RP structure embedded in a continuum random structure (respectively RP and FR structural components), as was already concluded in [9] for these aggregates.

2. Bhatia-Thornton partial structure factor

The partial structure factors introduced by Bhatia and Thornton [29] are associated with density and concentration correlations in binary alloys. They have been extended to alloys consisting of more than two components [30] and can then be used by considering random aggregates as alloys of spheres with various coordination numbers.

a. Formalism. The partial structure factor corresponding to the density-density correlation function S_{NN} is written

$$S_{NN}(Q) = 1 + \rho \int_0^\infty [P(r) - 1] \frac{\sin(Qr)}{Qr} 4\pi r^2 dr, \qquad (18)$$

to the concentration-concentration correlation function $S_{C_iC_j}$ is written

$$S_{C_iC_j}(Q) = 1 + \rho \int_0^\infty [-P(r) + P_i(r) + P_j(r) - P_{ij}(r)] \times \frac{\sin(Qr)}{Qr} 4\pi r^2 dr, \qquad (19)$$

and to the density concentration S_{NC_i} is written [10,21]

$$S_{NC_i}(Q) = \rho \int_0^\infty [P_i(r) - P(r)] \frac{\sin(Qr)}{Qr} 4\pi r^2 dr. \qquad (20)$$

For the sake of simplicity, we only consider hereafter sphere mixtures made of two components, namely, i and j coordinated spheres. The corresponding relations are provided in the Appendix.

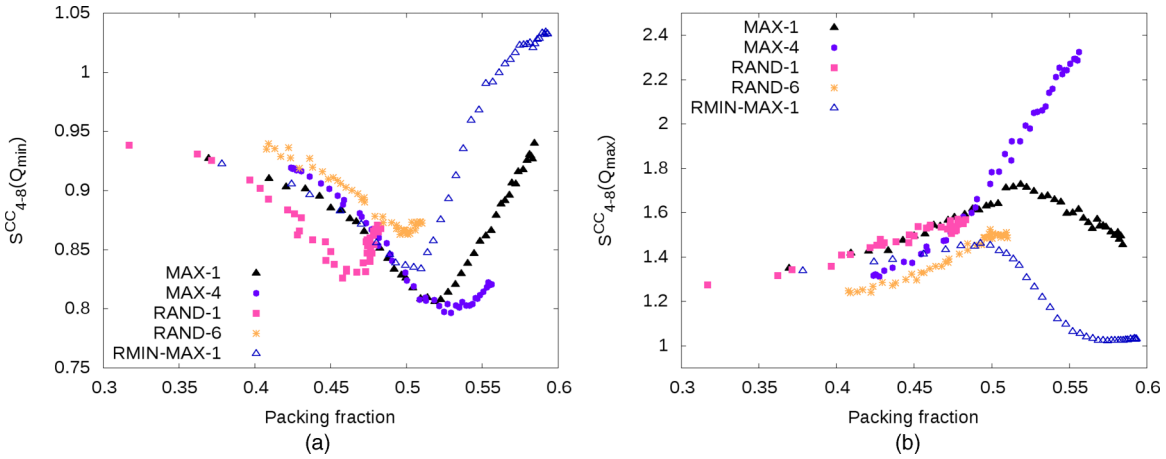

FIG. 19. (a) Amplitude of the S^{CC}_{4-8} minimum ($Q \in [1.7–1.9]$). (b) Amplitude of the small-Q maxima in Bhatia-Thornton S^{CC}_{4-8} structure factors ($Q < 1$).

b. Results. Between 15 (for high packing fraction) and 45 sets of Bhatia-Thornton (BT) structure factors corresponding to different coordination pairs i-j were calculated for 500 aggregates. In the case of high-packing-fraction aggregates where extreme coordination numbers (i.e., $i = 3$ and $i > 9$) are scarce, BT sets could only be calculated for coordination numbers lying between 4 and 8, hence the lower number of BT structure factors calculated for them.

A sample of Bhatia-Thornton partial structure factors is provided in the Appendix for three MAX-1 aggregates, with maximum, minimum, and intermediate packing fractions along with those of one RRPA. Their main characteristics are the following.

(i) The $S_{N_iN_j}$ structure factor is related to the overall structure of the two coordination numbers i and j considered. It looks like the average AL structure factor for small coordination differences ($i - j = 1$ or 2 at most), while it resembles more the global structure factor of the aggregate for "large" differences in coordination numbers ($i - j \geqslant 4$)

(ii) The S_{NC_i} structure factors exhibit significant oscillations whose intensity increases with the coordination difference $i - j$. Furthermore, for low coordination number differences these oscillations decrease when the coordination numbers increase. All these oscillations come from the fact that the average environment of spheres i and j characterized by P_i and P_j differ from the average global environments $P(r)$ [see the relation (20)]. This behavior differs completely from the case of binary substitution alloys (with equal atomic diameters) for which S_{NC} does not oscillate at all because $P_i(r) \approx P(r)$, independently of the chemical order of the two alloy components (which only affects S_{CC} [21]).

(iii) Most interesting is the study of $S_{C_iC_j}$, which characterizes the chemical order between i and j coordinated spheres through its dependence on $P_{ii} - P_{ij}$ [see Eq. (19)]. For small coordination differences (at most 2) and all packing fractions, $S_{C_iC_j}$ oscillates weakly around 1 and there is no chemical order effect between i and j coordinated spheres.

For large coordination differences ($i - j \geqslant 4$) a predepth is observed on S_{CC} around $Q \approx 0.5Q_1$. This predepth indicates a segregation effect [31], between spheres with large CCN differences. It varies nonuniformly with packing fraction [see Fig. 19(a)] and its maximum amplitude lies in the packing fraction interval $\gamma \in [0.5, 0.55]$. This segregation effect occurs over distances larger than contact neighbors, as it was suggested by the radial dependence of ⟨CCN⟩ seen in Sec. V A 3. As a matter of fact, the maximum segregation measured by this predepth occurs in a range of packing fraction where there is virtually no contact segregation in the case of RMIN-MAX-1 aggregates [by comparing Figs. 9(b) and 9(a)], suggesting that there can exist contact and longer-range segregation effects between spheres of various coordination numbers and that these two types of segregation are not necessarily concomitant.

Furthermore, for these high coordination differences a new S_{CC} prepeak appears at very-small-Q values, around $0.2Q_1$, which seems to vanish in the aggregates with the highest packing fraction [Fig. 19(b)], with the notable exception of MAX-4. Accordingly, this S_{CC} prepeak is also observed in the RRPA. This peak should be associated with the existence of segregation effects extending to the larger-r range, i.e., to the formation of isocoordinated aggregates in an average matrix. This suggests the existence of regions of low or high coordination in the aggregate matrix.

VI. DISCUSSION AND CONCLUSION

The so-called random packings of adhesive hard spheres cover a wide range of packing fractions, from a lower limit of 0.15 at the three-dimensional percolation threshold [32] with contact coordination number 2 [21] up to a maximum value of about 0.636 in the random close packing with coordination number approximately 8.1, as determined experimentally by Scott [33]. In this paper we focused on the detailed structural characterization of such packings, using a wide variety of static aggregate-building algorithms.

The randomness or isotropy of the 10^4 aggregates (containing 10^6 spheres each one) was checked first by studying the angular distribution of pairs of spheres separated by a given distance. The eigenvalues of the corresponding nematic order tensor were shown to be always less than 2×10^{-2} and confirmed that aggregates are fully isotropic.

Accurate methods for the determination of the aggregate packing fraction were then introduced. It was thus shown that

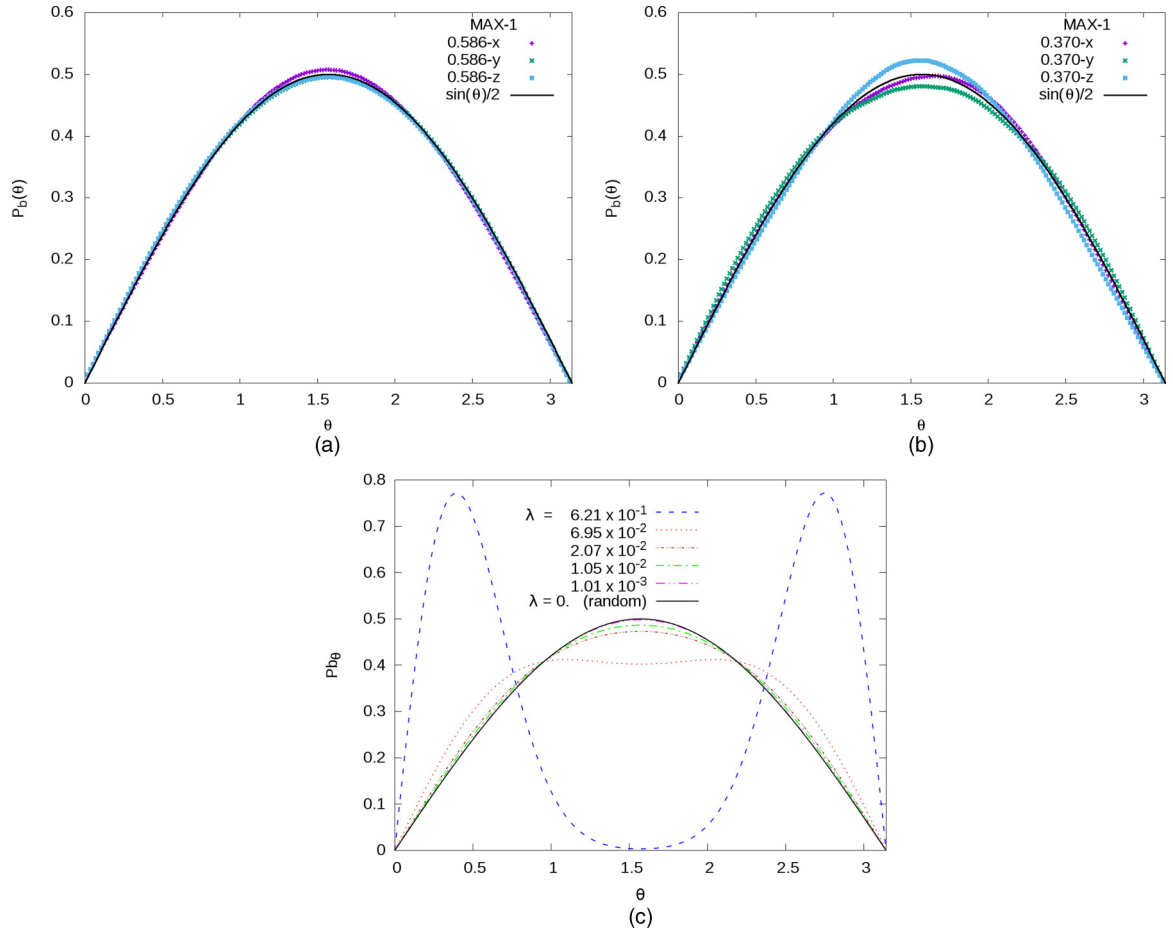

FIG. 20. Pair angle distributions with respect to x, y, and z for the (a) most and (b) least dense aggregates produced by the MAX-1 algorithm. (c) Polar angle distribution relative to the favorable direction in the uniaxial anisotropy case for different values of the nematic order parameter λ defined as the largest eigenvalue of the tensor $\bar{Q}$ [Eq. (A1)].

seed effects at the origin of the aggregates do not extend beyond the fifth-neighbor range, i.e., are limited to the first 8000 spheres, if the seed consists of sphere arrangements that are rare in the aggregate. This seed effect can be totally removed by using as the seed a sample with a structure similar to the built aggregate.

On the other hand, it has been shown that the effect of the imperfect spherical surface of the aggregates depends on the building algorithm and packing fraction and is limited to a thickness of approximately $6r_s$ in the worst case. Finally, the accuracy of the (average) packing fraction increases with the sphere number of the aggregate, which must reach 10^6 in order to get a 10^{-3} accuracy.

The detailed structural analysis of random packings could then be undertaken. As the first step, these structures were tackled via the Delaunay tessellation of tetrahedra connecting sphere centers. The distributions of these tetrahedra were characterized by two distortion parameters $L_{\max}$ and κ_D. Their distributions show a bimodal character that varies with packing fraction and appear related; they both include discontinuities whose origin remains unclear. Their average values decrease with increasing packing fraction. However, they provide complementary characterization of the aggregates produced by the various algorithms studied, suggesting that beyond their similarities, these distributions also present subtle differences.

Special attention was paid to the populations of regular tetrahedra (formed by four mutually contacting spheres, $L_{\max} = 2$) and quasiregular Delaunay tetrahedra ($L_{\max} < 2.3$) which were shown to behave quite differently. As a matter of fact, the volume fraction of regular tetrahedra has been shown to decrease with increasing packing fraction and reaches a maximum value of 0.165 for RPPAs (only built with regular construction tetrahedra). This raises a fundamental question: Is there a maximum geometrically defined (i.e., irrespective of their building mechanism) proportion of regular tetrahedra in random aggregates? Conversely, the proportion of quasiregular Delaunay tetrahedra goes to a minimum around $\gamma = 0.56$ and then increases with increasing packing fraction. Structural characterization methods could then be introduced by taking advantage of the unequivocal definition of sphere contacts and hence contact coordination numbers.

First, partial characterization was carried for short distances, i.e., contacting neighbors. The distributions of pairs of spheres with respective CCNs i and j (η_{ij}) were first studied. Their FWHM increases when packing fraction decreases and their average values $\langle \eta_{ij} \rangle$ show distinct behaviors with respect

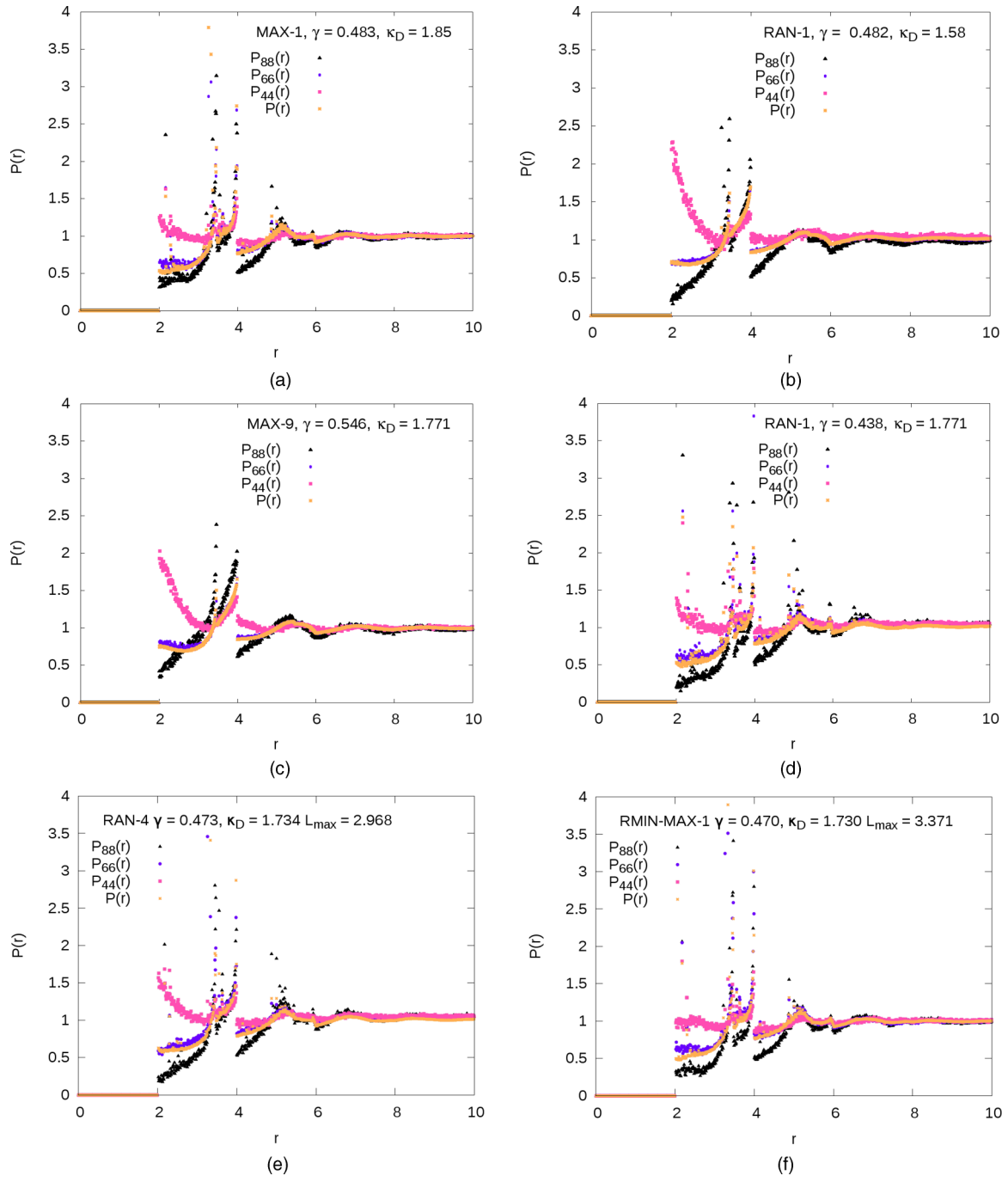

FIG. 21. Samples $P(r)$ and $P_{ii}(r)$ obtained for aggregates generated by the algorithms (a) MAX-1 ($\gamma = 0.483$), (b) RAN-1 ($\gamma = 0.482$), (c) MAX-9 ($\bar{\kappa}_D = 1.771$), (d) RAN-1 ($\bar{\kappa}_D = 1.771$), (e) RAN-4, and (f) RMIN-MAX-1.

to γ for low and high values of i, respectively: A nonuniform decrease with γ is obtained only in the case of low-i values. The evolution of these distributions shows that contact segregation can exist between spheres of various CCNs, whereas the evolution of $\langle$CCN$\rangle$ for spheres of various coordination shows that another segregation may exist, on the basis of CCNs, over a larger range. Partial distributions of bond angles for spheres with different CCNs were also studied. It was shown that high-CCN spheres tend to have a smoother distribution, whereas low-CCN spheres present a depletion of low angle bonds and have a higher proportion of high angle bonds. These differences are particularly distinct in high-packing-fraction aggregates.

This structural description was then extended to all distances by introducing the partial pair distribution functions $P_{ij}(r)$, i.e., the probability of finding a sphere with CCN i at a distance r from another sphere with CCN j (normalized to 1 for large r) and local packing fractions around i coordinated spheres. The different shapes and discontinuities of the $P_{ij}(r)$ curves were given and this detailed analysis allowed a clear-cut distinction between different random packing structures which cannot be distinguished by their packing fraction and/or κ_D

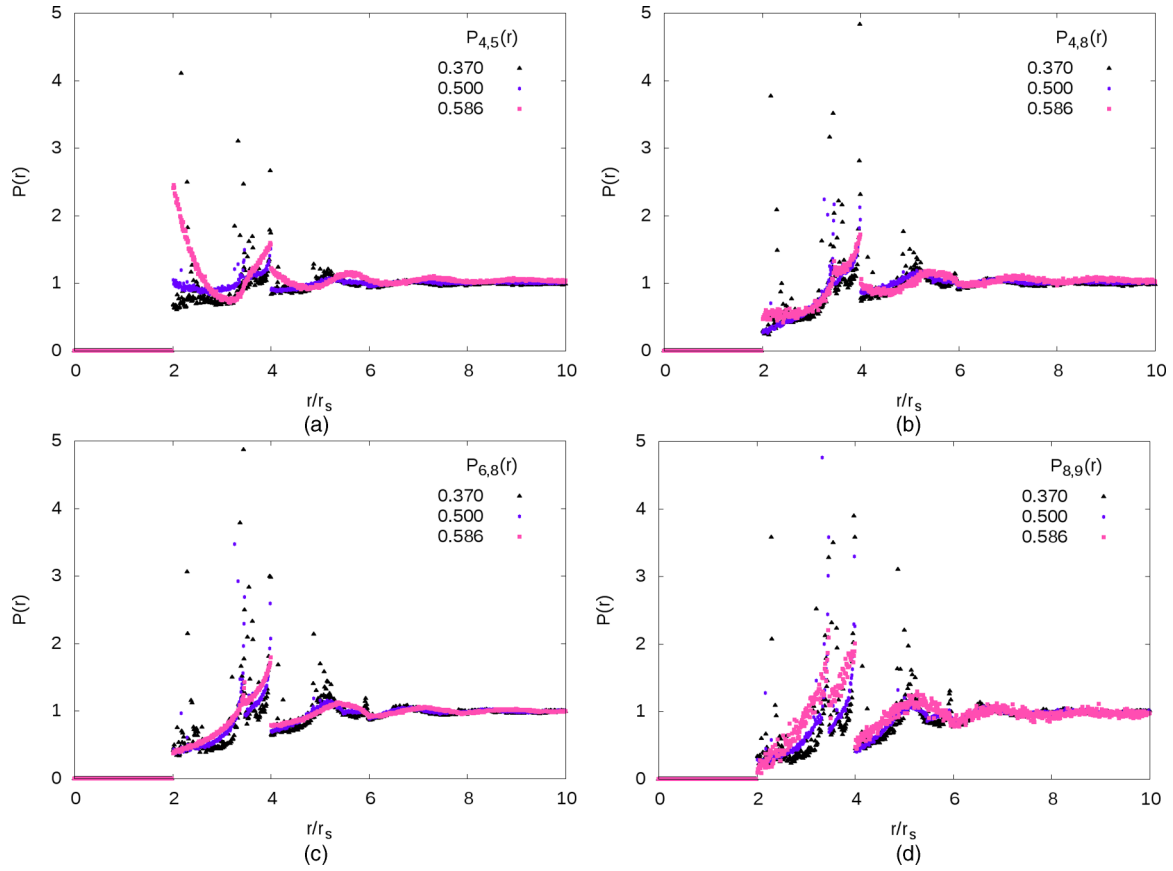

FIG. 22. Sample of $P_{ij}(r)$ for various packing fractions generated by the algorithm MAX-1: (a) $P_{4,5}(r)$, (b) $P_{4,8}(r)$, (c) $P_{6,8}(r)$, and (d) $P_{8,9}(r)$.

parameters. The question remains of whether these aggregates could be characterized by characterizing them through the combination of packing fraction γ and distortion parameter $L_{\max}$.

Distinguishing (with Refs. [34,35]) contacting from quasicontacting spheres, it was shown that high-CCN spheres have few quasicontacting neighbors (QCNs) while low-CCN spheres have a higher number of QCNs (as could be expected) and that this local effect extends to larger distances. Moreover, this behavior is amplified when the packing fraction increases.

Finally, the two sets of partial structure factors respectively introduced by Ashcroft-Langreth [$S_{ij}(Q)$] and Bhatia-Thornton (S_{NN}, S_{NC}, and S_{CC}) were analyzed. They are different Fourier transforms of linear combinations of the $P_{ij}(r)$ and can be directly compared with the results of diffraction experiments on liquid or disordered materials. In particular, the diagonal $S_{ii}(Q)$ give the partial structure factors of the partial aggregates made from i coordinated spheres and the variable shapes of these S_{ii}, especially their prepeak and first and second Q oscillations, were described. Furthermore, the concentration-concentration partial structure factor of Bhatia and Thornton gave the mutual or chemical order between spheres with different coordinations i and j and put forward heteroattractions or segregation of spheres within the different aggregates, confirming that several kind of segregation may indeed exist.

From all these results we could conclude that the random irregular polytetrahedral aggregates studied here are made from two basic components, namely, a fully random component (without regular tetrahedra) and a regular polytetrahedral component (only built with regular tetrahedra), whose proportion decreases with increasing packing fraction. This composite nature of the aggregates produces prepeaks (at very small Q) in the aggregate structure factors and the main features differentiating the RP component from the counterpart FR component are the following: a high proportion of regular Delaunay tetrahedra (as expected); an increase in δ peaks noticeable in distributions of Delaunay tetrahedra distortion indices, angular bond distributions, and global or partial pair distribution functions; an increase of the second mode in the distributions of Delaunay tetrahedra distortion parameters κ_D and $L_{\max}$; a spreading of contact coordination numbers distributions η_{ij}; strong variations in the radial dependence of the average contact coordination number of spheres; a collapse of the continuum of partial bond angle distributions; a more similar quasifirst-neighbor part of partial pair distribution functions of low- and high-contact-coordination-number spheres; a more similar radial dependence of packing fraction for spheres of any contact coordination number; a reduction of topological discontinuities in pair distribution function at $r = 2\sqrt{3}$ and 4; and a splitting of the structure factor's second peak ($Q \approx 7$), similar to what is experimentally found in amorphous tetrahedral materials.

The present results on statically built sticky-hard-sphere aggregates cover the packing fraction interval 0.370–0.593. It could be interesting to extend this study first to the low-packing-fraction range from 0.15 (condensation or percolation

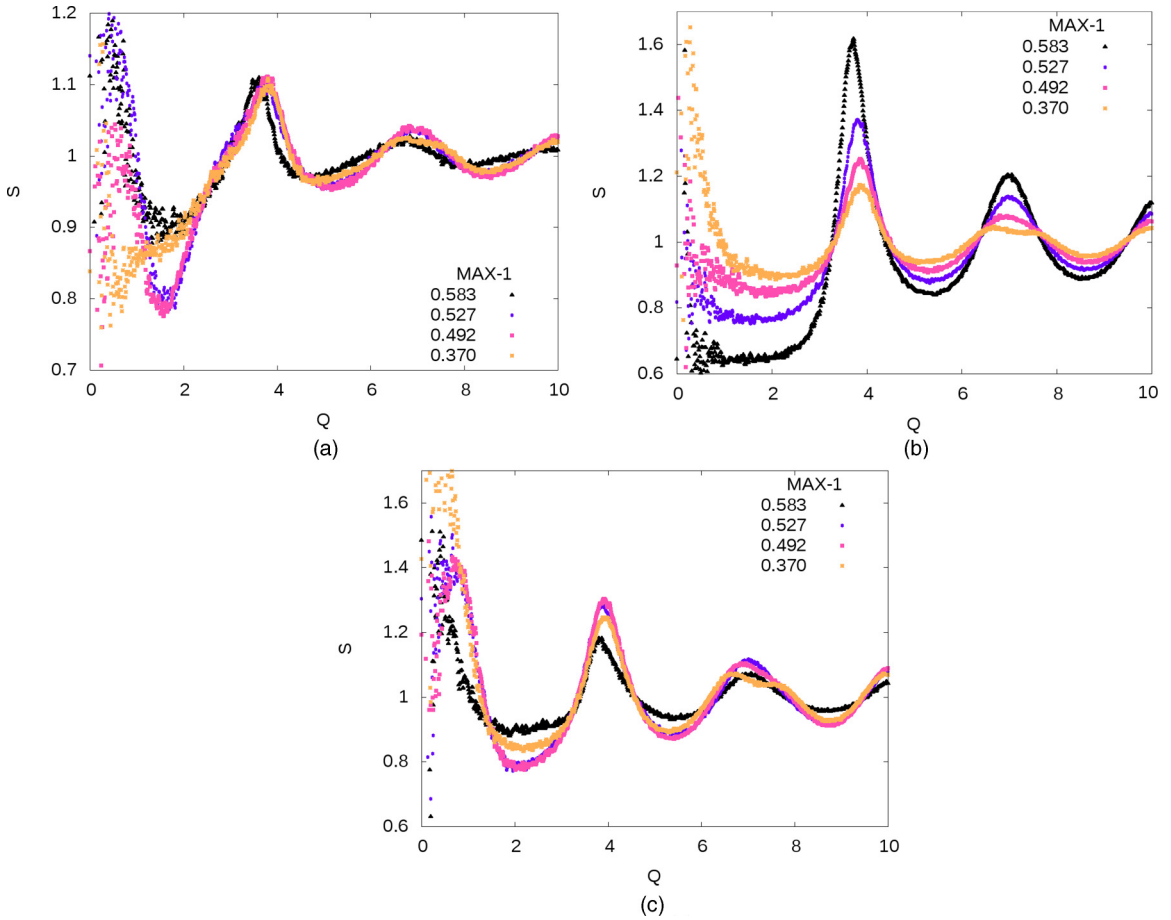

FIG. 23. Sample Ashcroft-Langreth structure factors for MAX-1 aggregates: (a) S_{44}, (b) S_{66}, and (c) S_{88}.

limit) to 0.370, which involves a contact coordination number lower than 3 and cannot be reached by the building algorithms used here, and second to the high-packing-fraction range 0.593–0.64, which needs a reduction of the fluctuations of the local packing fraction at all length scales and cannot be reached by our algorithms, which only minimize the fluctuations of the local packing fraction up to the second-neighbor distances. In particular, it would be of great interest to study dynamically built aggregates, such as the ones produced by the Lubachevsky-Stillinger algorithm, the Jodrey-Tory algorithm, or molecular dynamics. The first problem to be resolved would then be to define the distance corresponding to contacting spheres, as, for these aggregates, the first-neighbor peaks are spread over a finite length interval. Nonetheless, valuable structural information might be accessible through the techniques studied in the present work, which might shed light on various long-standing questions concerning random aggregates as well as allowing comparisons between statically and dynamically built random aggregates.

ACKNOWLEDGMENTS

P. Cénédèse is acknowledged for his help in openMP parallelization of some codes. Anonymous referees are thanked for their observations and suggestions that helped to improve the quality of this paper.

APPENDIX

Isotropic disordered aggregates are characterized by an isotropic distribution of $\hat{r}_{ij}$ bonds, where $\hat{r}_{ij}$ are the unit vectors joining the (i,j) sphere centers. This requirement provides a convenient check for the building method and/or the minimum aggregate size beyond which the isotropy is reached. Such a distribution is characterized by a uniform random distribution of azimuthal angles φ and a polar angles θ distribution following a probability density $P_b(\theta) = \sin(\theta)/2$. It is worth mentioning that a latticelike distribution of spheres is characterized by a θ distribution presenting distinguishable peaks; thus the features of the θ distribution appear to be a convenient tool to control both the aggregates randomness and isotropy.

In order to go beyond a simple qualitative characterization, we can quantify the deviation from isotropy by looking if a favored direction emerges throughout the $\{\hat{r}_{ij}\}$ distribution. For this, we follow the usual method of the framework of the nematic liquid statistics [36], according to which, from the diagonalization of the rank-2 tensor,

$$\bar{Q} = \frac{1}{N}\sum_{ij}\frac{1}{2}(3\hat{r}_{ij}\hat{r}_{ij} - \bar{I}), \tag{A1}$$

where $\bar{I}$ is the identity tensor and a nematic order parameter, say, S_1, is obtained as the largest eigenvalue $\lambda_{\max}$ of $\bar{Q}$. In Eq. (A1), the sum running over all the $\{i,j\}$ pairs can be limited

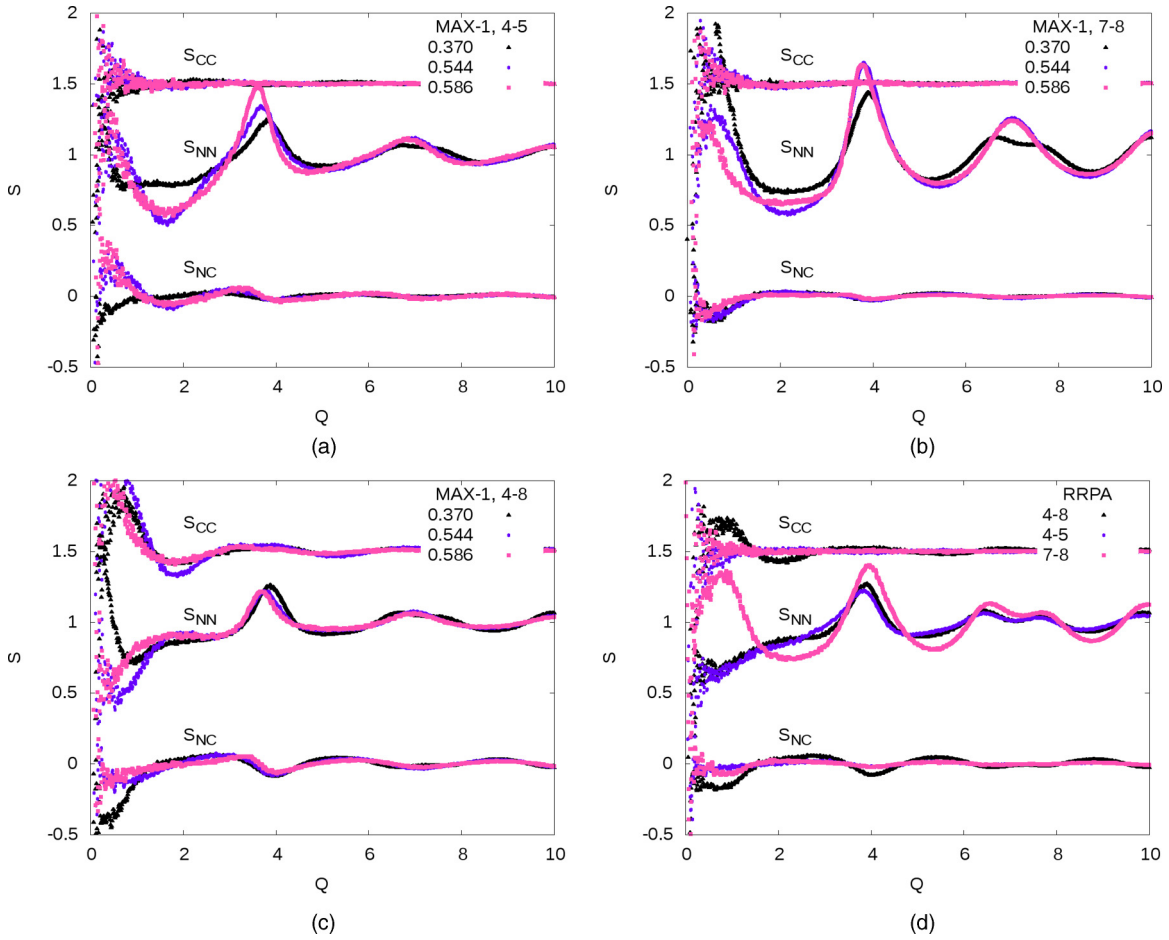

FIG. 24. Bhatia-Thornton partial structure factors for (a) 4-5, (b) 7-8, and (c) 4-8 for MAX-1 aggregates and (d) the RRPA. The S_{CC} oscillates around 1 but has been shifted to 1.5 for clarity.

to the sum over the bonds $\hat{r}_{ij}$, which can be replaced by a sum over the unit vectors carried by the $\vec{r}_i$, with respect to a fixed reference $\vec{r}_o$, which avoids the surface effects when both i and j are located at the aggregate surface.

The results for the polar angle distributions relative to the axes $\hat{x}$, $\hat{y}$, and $\hat{z}$ for the most and least dense aggregates obtained by the MAX-1 algorithm are presented, respectively, in Figs. 20(a) and 20(b). For the aggregates studied in this work, the deviation from isotropy as measured by the value of $\lambda_{\max}$ is found to decrease when the packing fraction increases. A reliable determination of the dependence of $\lambda_{\max}$ with respect to γ is beyond the scope of this paper, all the more that the range of $\lambda_{\max}$ values is quite small. The largest eigenvalue of $\bar{Q}$ is smaller than 3×10^{-2}. Such a value is very small, leading us to conclude that these building methods lead indeed to isotropic aggregates. To illustrate quantitatively this point, Fig. 20(c) displays the result of the θ distribution in terms of λ for the model

$$P_b(\theta) = \frac{\sin(\theta)}{2}[e^{(-\theta^2/2\sigma^2)} + e^{[-(\pi-\theta^2)/2\sigma^2]}], \tag{A2}$$

where the polar axis is a favored direction according to the variance σ. Clearly, the θ distributions characterized by λ values lower than a few 10^{-2} can be considered isotropic.

Figure 21 shows sample $P(r)$ and $P_{ii}(r)$ obtained for RIPA. Figure 22 shows a sample of $P_{ij}(r)$ for various packing fractions. Figure 23 shows sample AL structure factors. Figure 24 shows BT partial structure factors. General BT relations then reduce to

$$S_{N_iN_j}(Q) = 1 + \rho' \int \left(C_i'^2 P_{ii} + C_j'^2 P_{jj} + 2C_i'C_j' P_{ij} - 1\right) \times \frac{\sin(Qr)}{Qr} 4\pi r^2 dr, \tag{A3}$$

where $\rho' = (N_i + N_j)/V$ and $C_i' = N_i/(N_i + N_j)$,

$$S_{C_i'C_j'}(Q) = 1 + \rho' C_i' C_j' \int \{[P_{ii}(r) - P_{ij}(r)] + [P_{jj}(r) - P_{ij}(r)]\} \frac{\sin(Qr)}{Qr} 4\pi r^2 dr, \tag{A4}$$

$$S_{NC_i'}(Q) = \rho' C_j' \int [C_i' P_{ii}(r) - C_j' P_{jj}(r) + (C_j' - C_i') P_{ij}(r)] \times \frac{\sin(Qr)}{Qr} 4\pi r^2 dr. \tag{A5}$$

[1] B. Alder and T. Wainwright, Studies in molecular dynamics, J. Chem. Phys. **31**, 459 (1959).

[2] B. D. Lubachevsky and F. H. Stillinger, Geometric properties of random disk packings, J. Stat. Phys. **60**, 561 (1990).

[3] W. S. Jodrey and E. M. Tory, Computer simulation of close random packing of equal spheres, Phys. Rev. A **32**, 2347 (1985).
[4] N. Karayiannis and M. Laso, Monte Carlo scheme for generation and relaxation of dense and nearly jammed random structures of freely jointed hard-sphere chains., Macromolecules **41**, 1537 (2008).
[5] G. Y. Onoda and E. G. Liniger, Random Loose Packings of Uniform Spheres and the Dilatancy Onset, Phys. Rev. Lett. **64**, 2727 (1990).
[6] K. J. Dong, R. Y. Yang, R. P. Zou, and A. B. Yu, Role of Interparticle Forces in the Formation of Random Loose Packing, Phys. Rev. Lett. **96**, 145505 (2006).
[7] A. Anikeenko and N. Medvedev, Polytetrahedral Nature of the Dense Disordered Packings of Hard Spheres, Phys. Rev. Lett. **98**, 235504 (2007).
[8] R. Jullien, A. Pavlovitch, and P. Meakin, Random packings of spheres built with sequential models, J. Phys A: Math. Gen. **25**, 4103 (1992).
[9] M. Bletry and J. Bletry, Fluctuations, structure factor and polytetrahedra in random packings of sticky hard spheres, J. Non-Cryst. Solids **411**, 85 (2015).
[10] J. Blétry, Diffraction des neutrons polarisés par les phosphures de cobalt amorphes. interprétation par des modèles structuraux applicables au métaux et aux liquides, Ph.D. thesis, INPG, 1979.
[11] N. Medvedev and E. Pilyugina, Three-dimensional packing of perfect tetrahedra, in *Proceedings of the 5th International Symposium on Voronoi Diagrams in Science and Engineering (ISVD-2008)*, edited by K. Sugihara and D. Kim (Kiev: Inst. Math., Nat. Acad. Sci. Ukraine, 2008), pp. 144–156.
[12] E. W. Weisstein, Sphere-sphere intersection, a Wolfram web resource edition, MathWorld, available at http://mathworld.wolfram.com/Sphere-SphereIntersection.html
[13] L. E. Silbert, Jamming of frictional spheres and random loose packing, Soft Matter **6**, 2918 (2101).
[14] B. Delaunay, La sphère vide, in *Proceedings of the International Mathematical Congress, Toronto, 1924* (unpublished), pp. 695–700.
[15] CGAL, Computational Geometry Algorithms Library, available at http://www.cgal.org
[16] C. Jamin, S. Pion, and M. Teillaud, 3D triangulations, CGAL user and reference manual, version 4.9, 2016, available at http://doc.cgal.org/4.9/Manual/packages.html
[17] A. Anikeenko, N. Medvedev, and T. Aste, Structural and entropic insights into the nature of the random-close-packing limit, Phys. Rev. E **77**, 031101 (2008).
[18] M. Skoge, A. Donev, F. Stillinger, and S. Torquato, Packing hyperspheres in high-dimensional Euclidean spaces, Phys. Rev. E **74**, 041127 (2006).
[19] N. Karayiannis, K. Foteinopoulou, and M. Laso, The structure of random packings of freely jointed chains of tangent hard spheres, J. Chem. Phys. **130**, 164908 (2009).
[20] G. Fournet, Scattering functions for geometrical forms, Bull. Soc. Fr. Min. Crist. **74**, 39 (1951).
[21] J. Blétry, Sphere and distance models for binary disordered systems, Philos. Mag. B **62**, 469 (1990).
[22] J. G. Kirkwood and F. P. Buff, The statistical mechanical theory of solutions. I, J. Chem. Phys. **19**, 774 (1951).
[23] G. Etherington, A. C. Wright, J. T. Wenzel, J. C. Dore, J. H. Clarke, and R. N. Sinclair, A neutron diffraction study of the structure of evaporated amorphous germanium, J. Non-Cryst. Solids **48**, 265 (1982).
[24] P. Gaskell, A. Saeed, P. Chieux, and D. McKenzie, Neutron-Scattering Studies of the Structure of Highly Tetrahedral Amorphous Diamondlike Carbon, Phys. Rev. Lett. **67**, 1286 (1991).
[25] K. Laaziri, S. Kycia, S. Roorda, M. Chicoine, J. Robertson, J. Wang, and S. Moss, High Resolution Radial Distribution Function of Pure Amorphous Silicon, Phys. Rev. Lett. **82**, 3460 (1999).
[26] A. Narten, M. Danford, and H. Levy, X-ray diffraction study of liquid water in the temperature range 4–200°C, Discuss. Faraday Soc. **43**, 97 (1967).
[27] A. H. Narten, C. G. Venkatesh, and S. A. Rice, Diffraction pattern and structure of amorphous solid water at 10 and 77 °K, J. Chem. Phys. **64**, 1106 (1976).
[28] D. Polk, Structural model for amorphous silicon and germanium, J. Non-Cryst. Solids **5**, 365 (1971).
[29] A. Bhatia and D. Thornton, Structural aspects of the electrical resistivity of binary alloys, Phys. Rev. B **2**, 3004 (1970).
[30] J. Blétry, Partial structure factors in multicomponent liquid or amorphous alloys, Z. Naturforsch. A **31**, 960 (1976).
[31] J. Blétry, Geometrical models for liquid metals and alloys, Z. Naturforsch. Teil A **33**, 327 (1978).
[32] R. Zallen, *The Physics of Amorphous Solids* (Wiley, New York, 1983).
[33] G. Scott, Packing of spheres: Packing of equal spheres, Nature (London) **188**, 908 (1960).
[34] J. Bernal and J. Mason, Co-ordination of randomly packed spheres, Nature (London) **188**, 910 (1960).
[35] J. Bernal, The structure of liquids, Proc. R. Soc. London **280**, 299 (1962).
[36] R. D. Mountain and T. Ruijgrok, Monte-Carlo study of the Maier-Saupe model on square and triangle lattices, Physica A **89**, 522 (1977).